



CHORUS

This is the accepted manuscript made available via CHORUS. The article has been published as:

Accuracy of density functional theory in predicting formation energies of ternary oxides from binary oxides and its implication on phase stability

Geoffroy Hautier, Shyue Ping Ong, Anubhav Jain, Charles J. Moore, and Gerbrand Ceder

Phys. Rev. B **85**, 155208 — Published 30 April 2012

DOI: [10.1103/PhysRevB.85.155208](https://doi.org/10.1103/PhysRevB.85.155208)

Accuracy of Density Functional Theory in Predicting Formation Energies of Ternary Oxides from Binary Oxides and its Implication on Phase Stability

Geoffroy Hautier,* Shyue Ping Ong, Anubhav Jain, Charles J. Moore, and Gerbrand Ceder[†]
*Massachusetts Institute of Technology, Department of Materials Science and Engineering,
77 Massachusetts Avenue, 02139 Cambridge, MA, USA*

(Dated: April 2, 2012)

The evaluation of reaction energies between solids using density functional theory (DFT) is of practical importance in many technological fields and paramount in the study of the phase stability of known and predicted compounds. In this work, we present a comparison between reaction energies provided by experiments and computed by DFT in the generalized gradient approximation (GGA), using a Hubbard U parameter for some transition metal elements (GGA+ U). We use a data set of 135 reactions involving the formation of ternary oxides from binary oxides in a broad range of chemistries and crystal structures. We find that the computational errors can be modeled by a normal distribution with a mean close to zero and a standard deviation of 24 meV/atom. The significantly smaller error compared to the more commonly reported errors in the formation energies from the elements is related to the larger cancellation of errors in energies when reactions involve chemically similar compounds. This result is of importance for phase diagram computations for which the relevant reaction energies are often not from the elements but from chemically close phases (e.g., ternary oxides vs binary oxides). In addition, we discuss the distribution of computational errors among chemistries and show that the use of a Hubbard U parameter is critical to the accuracy of reaction energies involving transition metals even when no major change in formal oxidation state is occurring.

PACS numbers:

I. INTRODUCTION

Density functional theory (DFT) computations can provide the total energy of solid compounds. These total energies are then used to obtain reaction energies which are of importance in many fields such as batteries, hydrogen storage, Hg absorption, carbon capture or thermochemical water splitting.¹⁻⁸ Reaction energies are also critical to the *ab initio* study of the thermodynamic stability of known materials⁹⁻¹⁴ or the prediction of novel phases.¹⁵⁻²⁷ Indeed, it is a compound's energy relative to the energy from combinations of other phases, which determines its stability.

While comparisons between experimental and computed energies of reactions for solids exist in the literature, they tend to focus on very specific chemistries and/or crystal structures (e.g., perovskites^{28,29}). In contrast to the evaluation of molecular systems in the quantum chemistry field,^{30,31} there is a lack of statistically broad studies on the accuracy of specific DFT functionals in predicting energies of reactions between solid phases. This situation makes it difficult to add an error bar to predictions of reaction energies and can hinder the evaluation of the results provided by *ab initio* phase stability studies (i.e., the study of phase diagrams built from *ab initio* computations). Hence, the objective of this paper is to assess the accuracy of DFT in predicting reaction energies relevant to phase stability in multicomponent oxides by comparing, on a large data set, experimental and computed reaction energies from binary oxides to ternary oxides.

Our comparison between DFT and experimental reaction energies is mainly based on two very large experimental thermochemical data sources, the Kubachewski and the NIST databases.^{32,33} While it is common to report reaction energies from the elements, elemental reaction energies are not, in general, relevant to phase stability. Indeed, when one wants to determine if a predicted multicomponent compound is thermodynamically stable, the reaction energy determining the stability of the new compound is typically not with respect to the elements but to more chemically similar phases. For instance, the stability of a ternary oxide is most often determined by its relative energy versus other oxides (binaries and/or ternaries) and not versus the elements. In this work, we focus on the accuracy of the reaction energies that are relevant to the phase stability of ternary oxides with respect to binary oxides.

Using 135 of these solid phase reactions, we present in this paper the largest reported comparison between experimental and DFT computed solid phase reaction energies. We analyze the error distribution, and the chemistries for which errors are the most significant. Finally, we discuss the implication of our work on the evaluation of multicomponent phase diagrams obtained by GGA and GGA+ U . We stress that our study, by providing an error distribution for reaction energies involving chemically similar compounds, can be used to quantitatively assess the results obtained when computing the stability of new predicted phases with DFT.

II. METHODOLOGY

A. DFT parameters

The DFT computations were performed using a generalized gradient approximation (GGA) functional parametrized by Perdew, Burke and Ernzerhof (PBE).³⁴ The transition metals, Cu, Fe, Cr, Co, Mn, Ni, V, Nb, and Mo, were assigned a U parameter to correct for the self-interaction error present in GGA.^{35,36} This U parameter was fitted to experimental binary oxides formation energies using the Kubaschewski tables³² following the approach from Wang et al.³⁷ We excluded tungsten from our analysis due to the difficulty to fit a U value reproducing experimental enthalpies. All compounds were run with a k -point density of at least 500/(number of atom in unit cell) k -points. The Vienna *ab initio* software package (VASP)³⁸ was used with the provided projector augmented wave (PAW) pseudopotentials.³⁹ All pseudopotentials and U values are provided in Appendix A. With these parameters, the computations are expected to be converged to one meV/atom for oxide materials.⁴⁰ More details on the high-throughput *ab initio* methodology and parameters can be found in Jain et al.⁴⁰ All magnetic moments were initialized in a ferromagnetic (FM) state but compounds containing V, Mo, Cu, Nb, Co, Cr, Mn, Ni, and Fe, were also computed with an anti-ferromagnetic (AFM) state initialization. We computed all non-symmetrically equivalent AFM magnetic orderings in the smallest possible supercells using Hart’s algorithm.⁴¹ From all different FM and AFM initializations, the one with the lowest energy was chosen for our data set. For entries with mixed oxidation states (i.e., Fe_3O_4 and Mn_3O_4), we verified that charge ordering actually occurred in the GGA+ U computation.

In all cases, two full subsequent ionic relaxations were performed using the DFT parameters described above and the AFLOW wrapper around VASP.^{42,43}

B. Experimental data selection

Due to their relevance in technological applications and the large experimental data set available for ternary compounds, we only considered oxides in this study. For each oxide compound in the Kubaschewski tables,³² we searched for a corresponding crystal structure in the Inorganic Crystal Structure Database (ICSD).⁴⁴ Often the crystal system (e.g., monoclinic or cubic) or the mineral name is given in the Kubaschewski tables and we used this partial structure information to choose the corresponding ICSD entries among polymorphs. When the data provided by Kubaschewski was not sufficient to choose among polymorphs, we chose the lowest energy polymorph. The Kubaschewski entries that did not have a corresponding ICSD entry were disregarded, as were compounds with partial occupancies.

To exclude as much as possible unreliable experimental data from our study, we double-checked the formation enthalpies provided by Kubaschewski versus other sources (the NIST database,³³ the Landolt-Bornstein database,⁴⁵ the CTDTP database,⁴⁶ and the scientific literature). The principal verification was performed against the NIST database³³ which contains less data (especially for ternary oxides) but provides more recent and accurate data than the Kubaschewski tables. We found 107 oxide entries in the Kubaschewski table having an equivalent entry in the NIST database. If the difference in enthalpy between the two pieces of data was higher than 5 meV/atom, we chose the NIST value. This situation occurred for nineteen entries in our data and the largest differences (≥ 30 meV/atom) were found for six entries: Mg_2TiO_5 (216 meV/atom), K_2SiO_3 (72 meV/atom), Be_2SiO_4 (43 meV/atom) and CuO (30 meV/atom). The remaining entries in Kubaschewski for which no NIST data is available were compared with the information in the Landolt-Bornstein database.⁴⁵ For the entries with large discrepancies (≥ 20 meV/atom in formation enthalpy), we looked for a third source to determine whether the value from the Kubaschewski or Landolt-Bornstein database should be used. We had to exclude four compounds (Cs_2SiO_3 , K_3PO_4 , Li_3AsO_4 , and BaV_2O_6) because of the lack of a reliable third source, and we selected the value from the Landolt database for four other compounds (FeMoO_4 , $\text{Na}_4\text{V}_2\text{O}_7$, Na_2MoO_4 and KFeO_2). The remaining entries (without data in NIST and Landolt-Bornstein) were compared to the CTDTP database. The eight entries in the CTDTP database were all in agreement (within 20 meV/atom) with the Kubaschewski data. Finally, the remaining 14 compounds (without data in NIST, Landolt-Bornstein and CTDTP) were compared to values found in the literature. Seven had to be excluded from our data set as no consistent data was found in the literature (SrB_4O_7 , LiTaO_3 , LiNbO_3 , LaPO_4 , LiB_3O_5 , NaVO_3 , and CdTiO_3).

Each enthalpy of formation in the Kubaschewski table is given with an experimental error. Assuming that the experimental errors on enthalpies of formation are normally distributed and independent, the error on a reaction enthalpy (which is the result of a sum of enthalpy of formations) can be computed using the rule of summation of normally distributed random variables. The resulting error on the reaction energy is also normally distributed, with a standard deviation of $\sigma_{reaction} = \sqrt{\sum_i a_i^2 \sigma_i^2}$. The σ_i represent the standard deviation associated with the experimental enthalpy of formation of each compound involved in the reaction, and a_i are the stoichiometric coefficients associated

with the product i in the reaction. For the few entries without any experimental error provided in the Kubachewski table, the Landolt database, or the literature, we attributed an error of 10 meV/atom corresponding to the average experimental error in the Kubachewski tables. We attributed an experimental error of 5 meV/atom for the more reliable NIST data.

C. Evaluating zero K energies from 298K enthalpies

The Kubachewski tables provide enthalpies of formation at 298K while the computed total energies refer to energies at zero K. To obtain experimental enthalpies at zero K, one needs to integrate the heat capacity between zero K and 298K. The experimental heat capacity of each compound is often provided in thermochemical tables as a polynomial expansion on the temperature and it is tempting to directly integrate the polynomial to zero K. However, this polynomial expansion is only valid for temperatures above 298K. Hence, we instead fit a Debye-like equation to the heat capacity at 298K with the additional constraint that the integration of this heat capacity divided by the temperature should give the formation entropy (also provided in the thermochemical tables) at 298K. The heat capacity at constant pressure (c_p) and per atom of compound is assumed to follow the Debye form:

$$c_p(T; T_D, A) = A \left(\frac{T}{T_D}\right)^3 \int_0^{\frac{T}{T_D}} \frac{x^4 e^x}{(e^x - 1)^2} dx \quad (1)$$

Where T_D , the Debye temperature, and A are constants. The constants A and T_D are determined for each compound from the heat capacity at 298K, $c_{p,298K}$, and the entropy at 298K, S_{298K} , provided in the Kubachewski tables:

$$c_p(298, T_D, A) = c_{p,298K} \quad (2)$$

$$\int_0^{298} \frac{c_p(T; T_D, A)}{T} dT = S_{298K} \quad (3)$$

Integrating the Debye model in equation (1) with the fitted A and T_D leads to the experimental enthalpy at zero K.

$$H_{0K} \simeq H_{298K} - \int_0^{298} c_p(T; A, T_D) dT \quad (4)$$

We compared our fitted Debye model to actual heat capacity measurements down to zero K for a few compounds, and found good agreement (see Appendix B).

As the heat capacity integration component depends on the entropy and heat capacity value provided by the Kubachewski tables, we compared them to the NIST database. We did not find any large differences except for the NaAlO_2 entropy for which we used the NIST values. For Fe_2ZnO_4 , we used direct values from the heat capacity integration provided in King et al.⁴⁷ as the heat capacity reported in the Kubachewski tables is unphysical and negative.

In addition, we neglect the pressure times volume (PV) term, assuming that the formation *energy* at zero K is equal to the formation *enthalpy* at zero K. When considering reaction energies between solids, the PV term of the enthalpy is negligible. We also neglect the zero-point energy (ZPE) contribution to the energy (typically less than a few meV/atom).^{48,49}

We provide in Appendix C for each compound the corresponding ICSD number, the experimental enthalpy of formation from the elements at zero K, the experimental error, the source of the enthalpy data (Kubachewski, NIST or Landolt) as well as the DFT (GGA and GGA+ U) total energy obtained by ionic relaxation. We also provide as supplementary materials the relaxed structures (in FM state) for each of the selected compounds to facilitate future comparison of our data set to other functionals or computational approaches.⁵⁰

D. Reaction energy critical to phase stability

When considering an $A_xB_yC_z$ compound in an A-B-C chemical system, there are many different reaction energies forming this compound that can be defined. Most often, the formation energy from the elements (e.g., $A + B + 2C \rightarrow ABC_2$) is reported but other reactions can be defined as well, for instance from binaries to ternaries (e.g., $\frac{1}{2}A_2C + \frac{1}{2}B_2C_3 \rightarrow ABC_2$) or even between ternaries and binaries (e.g., $\frac{1}{5}A_5BC_4 + \frac{2}{5}B_2C_3 \rightarrow ABC_2$). In this work, we present a method to choose the reaction most relevant to phase stability for a given $A_xB_yC_z$ phase. The algorithm relies on the convex hull construction. The convex hull construction effectively evaluates the stability of a given compound against any linear combination of compounds that have the same averaged composition, and is the common procedure to assess if a compound is stable versus the decomposition to other products. First, we construct the convex hull with all phases existing in the A-B-C, including all elemental, binary and ternary phases with the exception of the targeted $A_xB_yC_z$ phase. Then, we detect what phases constitute the equilibrium triangle in which the $A_xB_yC_z$ composition lies. The reaction from these phases in the equilibrium triangle to form the $A_xB_yC_z$ phase is defined as the reaction critical to phase stability. Indeed, it is this reaction that determines directly if the $A_xB_yC_z$ phase is stable (i.e., on the convex hull) or not (i.e., above the convex hull) as it compares the $A_xB_yC_z$ phase to the most competitive combination of phases. Figure 1 illustrates this algorithm for an hypothetical A-B-C system and a ABC_3 ternary phase. Using the phase diagram built by the convex hull construction without the ABC_3 phase, we can see that the ABC_3 composition (blue dot) lies in the triangle formed by the A_2C , BC_3 and BC_2 phases (the decomposition is indicated by the blue arrows). The critical reaction energy to phase stability is therefore $\frac{1}{2}A_2C + \frac{1}{2}BC_3 + \frac{1}{2}BC_2 \rightarrow ABC_3$. While we illustrated the method by using examples from ternary phase diagrams, the algorithm is easily generalizable to higher component systems (e.g., quaternaries) by considering the relevant equilibrium simplices.

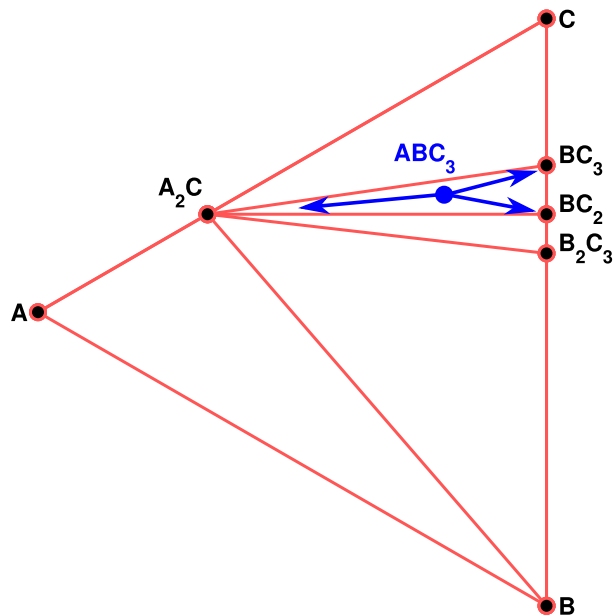


FIG. 1: (Color Online) Illustration of the procedure to determine the reaction critical to phase stability for a ABC_3 compound. By building the phase diagram using the convex hull construction on all phases in the A-B-C system with the exception of ABC_3 , we find that the equilibrium triangle consists in A_2C , BC_3 and BC_2 . The critical reaction energy to phase stability is therefore $\frac{1}{2}A_2C + \frac{1}{2}BC_3 + \frac{1}{2}BC_2 \rightarrow ABC_3$.

We applied this algorithm to determine what would be the critical reaction energy from binary to ternary oxides for each ternary oxide present in our data set. For chemical systems including only cations with single oxidation states, there is only one binary oxide to ternary oxide reaction that needs to be considered. For instance, in the case of $LiAlO_2$, the only reaction energy forming this ternary compound from binary oxides is $\frac{1}{2}Al_2O_3 + \frac{1}{2}Li_2O \rightarrow LiAlO_2$. On the other hand, when a ternary oxide contains elements forming in several oxidation states (e.g., $CoFe_2O_4$), there is more than one reaction involving binary oxides reacting to form the ternary compound, but only one reaction will be directly critical to the phase stability of the ternary (i.e., $CoO + Fe_2O_3 \rightarrow CoFe_2O_4$). If any of the competing phases is a gas (e.g., CO_2 for a carbonate or SO_2 for a sulfate), the ternary oxide was not considered in our data set. Gases

were excluded from our analysis because of the large known errors in DFT associated with molecular species (e.g., oxygen molecule overbinding).^{37,51}

In total, our data set consists of 135 reaction energies and each computed and experimental reaction energy is present in Appendix C. In this work, we will express all reaction energies as energy per atom of ternary compound (eV/atom or meV/atom); 10 meV/atom corresponds to about 1 kJ/mol-atom.

III. RESULTS

Figure 2 plots the experimental reaction energies as a function of the computed reaction energies. All reactions involve binary oxides to ternary oxides and have been chosen as presented in the Methods section. The error bars indicate the experimental error on the reaction energy. The data points follow roughly the diagonal and no computed reaction energy deviates from the experimental data by more than 150 meV/atom. Figure 2 does not show any systematic increase in the DFT error with larger reaction energies. This justifies our focus in the present study on absolute and not relative errors.

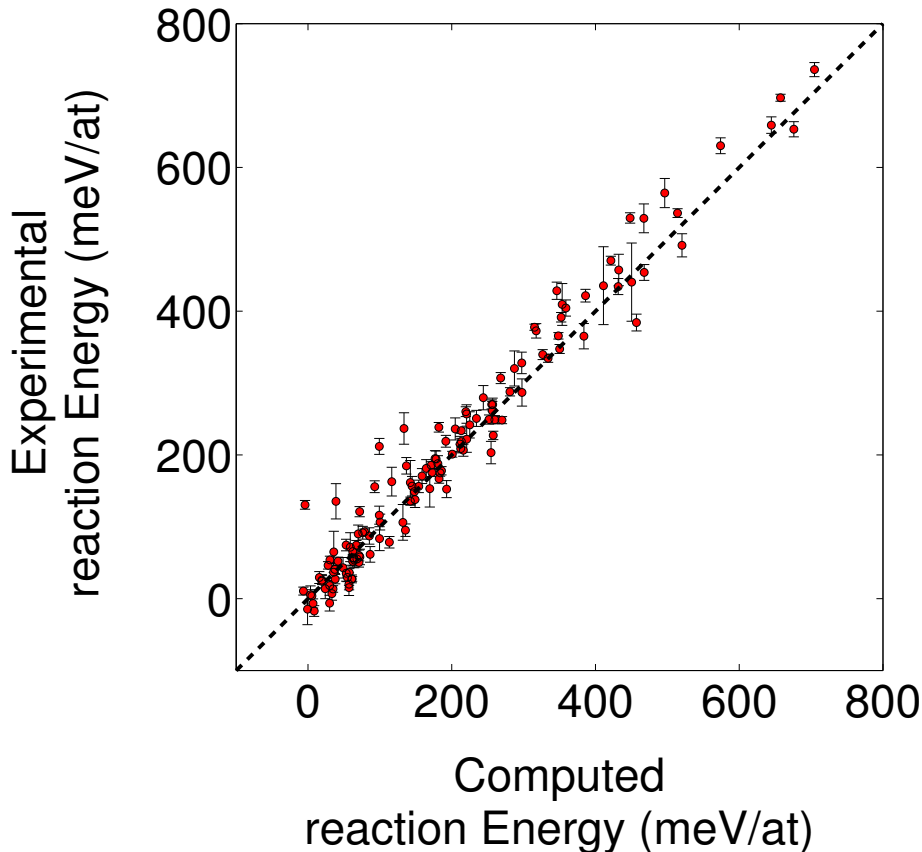


FIG. 2: (Color Online) Experimental reaction energy as function of the computed reaction energy (in meV/atom). The error bar indicates the experimental error. As the reaction energies are typically negative, the graph actually plots the negative of the reaction energy.

In Figure 3, we plot a histogram of the difference between the DFT and experimental reaction energies. GGA+ U underestimates and overestimates the energy of reaction with the same frequency, and the mean difference between computed and experimental energies is 9.6 meV/atom. The root mean square (rms) deviation of the computed energies with respect to experiments is 34.4 meV/atom. Both the mean and rms are very different from the results obtained by Lany on reaction energies *from the elements*.⁵² Using pure GGA, Lany found that elemental formation energies are underestimated by GGA with a much larger rms of 240 meV/atom. Our results are closer to experiments because of the greater accuracy of DFT when comparing chemically similar compounds such as binary and ternary

oxides due to errors cancellation.⁴⁰ We should note that even using elemental energies that are fitted to minimize the error versus experiment in a large set of reactions, Lany reports that the error is still 70 meV/atom and much larger than what we find for the relevant reaction energies. The rms we found is consistent with the error of 3 kJ/mol-at (30 meV/atom) for reaction energies from the binaries in the limited set of perovskites reported by Martinez et al.²⁹

Very often, instead of the exact reaction energy, one is interested in knowing if a ternary compound is stable enough to form with respect to the binaries. This is typically the case when a new ternary oxide phase is proposed and tested for stability versus the competing binary phases.¹⁸ From the 131 compounds for which reaction energies are negative according to experiments, all but two (Al_2SiO_5 and CeAlO_3) are also negative according to computations. This success in predicting stability versus binary oxides of known ternary oxides can be related to the very large magnitude of reaction energies from binary to ternary oxides compared to the typical errors observed (rms of 34 meV/atom). Indeed, for the vast majority of the reactions (109 among 131), the experimental reaction energies are larger than 50 meV/atom. It is unlikely then that the DFT error would be large enough to offset this large reaction energy and make a stable compound unstable versus the binary oxides.

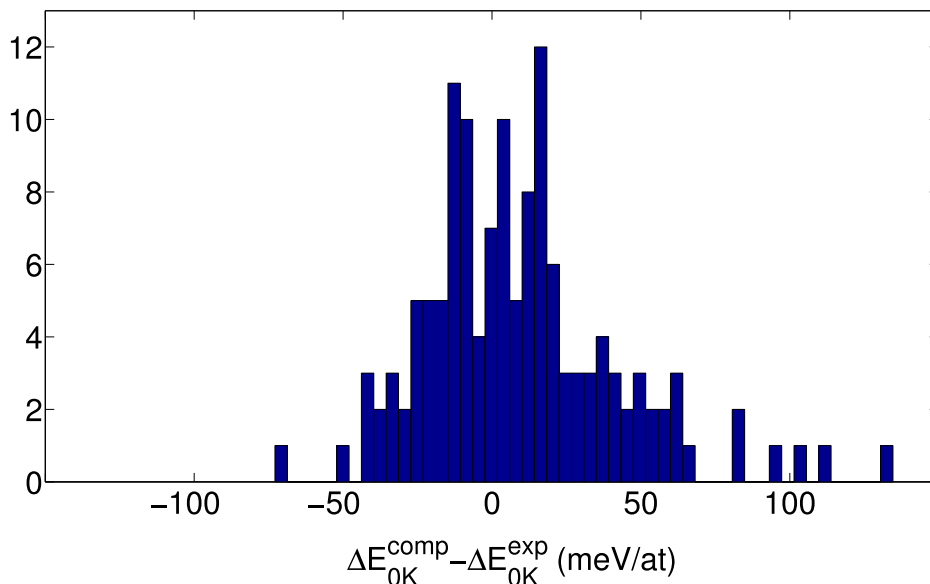


FIG. 3: (Color Online) Histogram of the difference between computed (ΔE_{0K}^{comp}) and experimental (ΔE_{0K}^{exp}) energies of reaction (in meV/atom).

The histogram in Figure 3 shows several reaction energies with significant errors. Failures and successes of DFT are often known to be chemistry dependent, and we present the effect of the chemistry on the DFT error by plotting, in Figure 4, a matrix of absolute reaction energies errors. The x axis represents the oxides of element A and the y axis the oxide of element B. Each element in the matrix corresponds to an A-B-O chemical system. When several reaction energies are available in a chemical systems (i.e., several ternary compounds are present), we plotted the maximum absolute error energy in this system. The matrix is symmetric as A-B-O is equivalent to B-A-O. The elements are sorted by their Mendeleev number⁵³ so that important chemical classes (e.g., alkalis or transition metals) are grouped together. The first row and column in the matrix indicate the mean of the difference computed experimental for one given element across all ternary oxide chemistries.

It is remarkable that no systematically larger error is present for elements with partially filled d -orbitals (e.g., Fe, Mn, Co or Ni), which indicates that the use of a Hubbard U is sufficient to compensate the error associated with the localized d -orbitals. On the other hand, elements containing f -electrons such as cerium show very large deviations from experiments. Both reaction energies involving cerium (i.e., related to $\frac{1}{2} \text{Ce}_2\text{O}_3 + \frac{1}{2} \text{Cr}_2\text{O}_3 \rightarrow \text{CeCrO}_3$ and $\frac{1}{2} \text{Ce}_2\text{O}_3 + \frac{1}{2} \text{Al}_2\text{O}_3 \rightarrow \text{CeAlO}_3$) disagree by extremely large values (around 130 meV/atom) from the experimental data. We should note that, in this study, we did not use any U value on f -orbitals and those Ce^{3+} compounds have a $4f^1$ electronic configuration with one f -electron participating in the bonding. This f -electron is poorly represented by GGA as Ce_2O_3 , CeCrO_3 and CeAlO_3 are computed to be metallic while they are in reality insulators. It is likely that

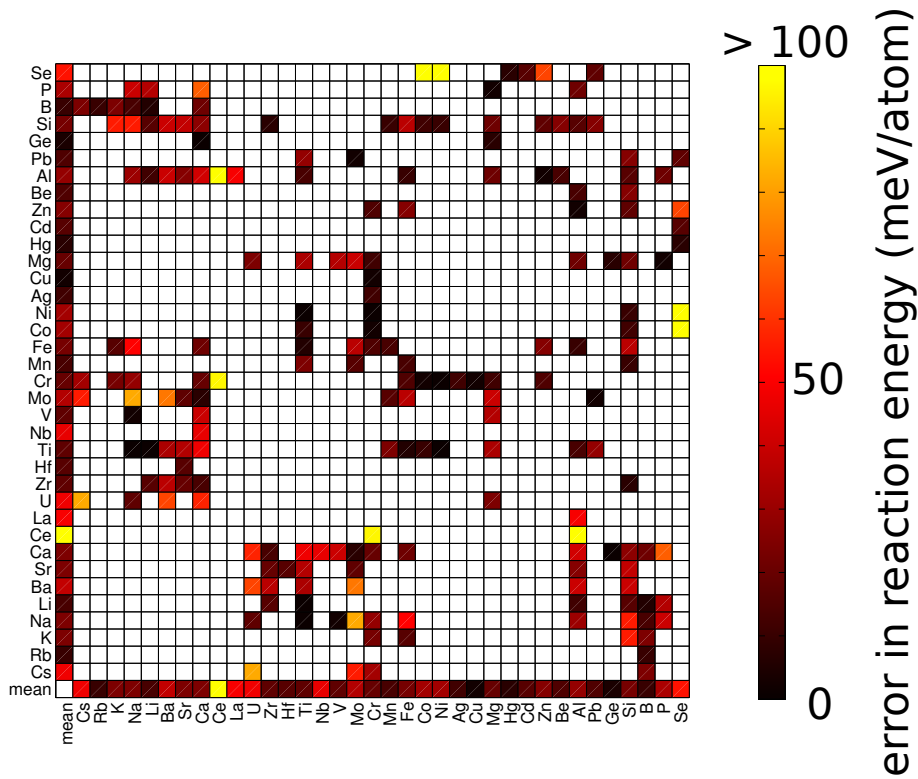


FIG. 4: (Color Online) Matrix of the difference between computed and experimental energies of reaction ($|\Delta E_{0K}^{comp} - \Delta E_{0K}^{exp}|$). The x (y) axis represents the oxides of element A (B). Each element in the matrix corresponds to a chemical system A-B-O. When several reaction energies are available in a chemical systems (i.e., several ternary compounds are present), we plot the maximum absolute error energy in this system. The matrix is symmetric as A-B-O is equivalent to B-A-O. The elements are sorted by Mendeleev number and the first row indicates the mean of the difference across the different chemistries.

this incorrect representation of the electronic structure explains the large discrepancy obtained in reaction energies for Ce^{3+} oxides. The difficulty to correctly model the electronic structure of Ce_2O_3 with GGA had already been pointed out by Skorodumova et al.⁵⁴ One proposed solution has been to apply a Hubbard U on the cerium f -electrons.⁵⁵ While fitting a U value for Ce is beyond the scope of this work, we indeed observe the reaction energy getting closer to the experimental data by applying a moderate U value ($U = 3$ eV) on the f electrons in Ce for both CeCrO_3 and CeAlO_3 (see Table I). The other f -containing elements (i.e., U and La) do not show as large discrepancies as Ce (with the exception of one uranium based compound Cs_2UO_4). This observation can be easily rationalized by the non-occupied character of the f -orbitals in the specific oxidation states of these uranium and lanthanum compounds (i.e., U^{6+} and La^{3+} do not have any occupied f electron states).

Reaction	Computed Energy without U on f-orbitals (meV/at)	Reaction Energy with U on f-orbitals (meV/at)	Experimental Energy (meV/at)
$\frac{1}{2} \text{Ce}_2\text{O}_3 + \frac{1}{2} \text{Cr}_2\text{O}_3 \rightarrow \text{CeCrO}_3$	-38.9	-52.2	-135
$\frac{1}{2} \text{Ce}_2\text{O}_3 + \frac{1}{2} \text{Al}_2\text{O}_3 \rightarrow \text{CeAlO}_3$	4.19	-50.9	-130

TABLE I: Comparison between the reaction energies from binary oxides to Ce-containing ternary oxides from experiment, computed with GGA (without a U applied on the f -orbitals in Ce) and with a U applied on f -orbitals in Ce. The U value for Ce was not optimized and set arbitrarily to 3 eV.

Another chemistry-dependent effect is the importance of a relativistic treatment, as effects due to spin-orbit coupling will be larger for heavier elements (e.g., Pb). Recently, Ahuja et al. showed that spin-orbit coupling is required to accurately reproduce certain reaction energies in lead-containing compounds.⁵⁶ The reaction energies studied by Ahuja

et al., involved a metal and two oxides with different oxidation states. Our simpler reactions (involving only oxides in a Pb^{2+} oxidation state) do not show major errors with lead-containing compounds (see Figure 4 and Table II). We should note, however, that spin-orbit coupling is incorporated indirectly in our computations in the construction of the PAW pseudopotentials.

Reaction	Computed (meV/at)	Experimental (meV/at)	Difference (meV/at)
$\text{TiO}_2 + \text{PbO} \rightarrow \text{PbTiO}_3$	-36	-65	29
$\text{SeO}_2 + \text{PbO} \rightarrow \text{PbSeO}_3$	-177	-195	18
$\text{MoO}_3 + \text{PbO} \rightarrow \text{MoPbO}_4$	-154	-156	2
$\text{SiO}_2 + \text{PbO} \rightarrow \text{PbSiO}_3$	-55	-29	25
$\text{SiO}_2 + 2\text{PbO} \rightarrow \text{Pb}_2\text{SiO}_4$	-37	-40	3

TABLE II: Experimental and computed reaction energies (in meV/atom) for lead-containing compounds.

Two molybdenum-based compounds (BaMoO_4 and $\text{Na}_2\text{Mo}_2\text{O}_7$) also show large errors (-72.9 and 82.2 meV/atom). While the thermochemical data for both these compounds is consistent in the Kubachewski and Landolt databases, a more refined literature search indicated that the discrepancy is due to measurements errors for both databases. The formation energy from the elements for $\text{Na}_2\text{Mo}_2\text{O}_7$ is reported from two different methods at -2245 and -2248.5 kJ/mol,^{57,58} while the Kubachewski data reports -2361 kJ/mol. Similarly, three literature references indicate a value around -1546 kJ/mol for the formation energy from the elements for BaMoO_4 ,⁵⁹⁻⁶¹ in contradiction with the value in the Kubachewski of -1516.3 kJ/mol. For both compounds, these revised values from the literature lead to closer agreement with the computed data (respectively -26 meV/atom and -22 meV/atom differences). Some selenate compounds in our data set show large deviations as well. The discrepancies are especially large for NiSeO_3 and CoSeO_3 (respectively 113 and 105 meV/atom) but also for ZnSeO_3 (63 meV/atom). The three other selenate compounds (HgSeO_3 , PbSeO_3 and CdSeO_3) do not show unusual errors. After a more detailed study, we found that Olin considered both experimental results from Ni and Co uncertain enough to exclude them from his comprehensive review on selenates.⁶² Olin confirms on the other hand the value provided by Kubachewski for ZnSeO_3 . Finally, a surprising large discrepancy is present for $\text{Ca}_3(\text{PO}_4)_2$ (67.9 meV/atom) and further investigation in the literature showed that the $\text{Ca}_3(\text{PO}_4)_2$ composition forms two polymorphs: an α and β phase. Both phases form in the rhombohedral crystal system and cannot be discriminated from the information present in the Kubachewski tables but enthalpy data from another source showed that the enthalpy provided by Kubachewski most likely relates to the β -phase.⁶³ In our work, we selected the α -phase because of the absence of crystallographic data with full occupancies for the β -phase in the ICSD. Using a simple ordering algorithm combined with an electrostatic energy model to select an ordering,⁴¹ we estimate the β -phase to be 32 meV/atom lower in energy than the α -phase. Using the ordered β -phase, the computed value is in better agreement with experiment (35.9 meV/atom difference).

Our data can be used to fit a probability distribution of the DFT errors. The simplest model would be to consider that the computational error is distributed normally with mean μ and standard deviation σ . Some of the large outliers discussed previously (i.e., BaMoO_4 , $\text{Na}_2\text{Mo}_2\text{O}_7$, $\text{Ca}_3(\text{PO}_4)_2$, and the nickel and cobalt selenates) are due to errors external to DFT (inaccurate enthalpy measurements or structure assignment), and we will exclude them for the rest of the analysis. Likewise, we excluded the cerium-based compounds as those errors could likely be fixed by using an adequate U value on f -electrons. In addition, the Kubachewski tables provide for each enthalpy of formation an estimate of the experimental accuracy of the measurement that needs to be deconvoluted from the error due to DFT. The difference between experimental and computed energy for a reaction i can be represented by a random variable X_i , that is the sum of the experimental error X_i^{exp} and the DFT error X_i^{DFT} .

$$X_i = X_i^{exp} + X_i^{DFT} \quad (5)$$

Assuming that the experimental error for the reaction i is distributed normally with zero mean and a standard deviation equal to σ_i (computed from the error bar on the formation energy of all compounds participating in the reaction as presented in the Methods section) and that the error between DFT and experiment is distributed normally as well with a mean μ and a standard deviation σ , we can show that

$$X_i = N(0, \sigma_i) + N(\mu, \sigma) \quad (6)$$

$$= N(\mu, \sqrt{\sigma^2 + \sigma_i^2}) \quad (7)$$

$$= \frac{1}{\sqrt{2\pi(\sigma^2 + \sigma_i^2)}} e^{-\frac{(x_i - \mu)^2}{2(\sigma^2 + \sigma_i^2)}} \quad (8)$$

The unknown parameters to evaluate are the mean and standard deviation of the DFT error (μ and σ). These two parameters can be estimated by a maximum likelihood approach.⁶⁴ The log-likelihood L for the n observations (i.e., the n reaction energies) can be expressed as

$$L = \log\left(\prod_{i=1}^n p(X_i = x_i)\right) \quad (9)$$

$$= \sum_{i=1}^n -\frac{(x_i - \mu)^2}{2(\sigma^2 + \sigma_i^2)} - \frac{1}{2} \sum_{i=1}^n \log(2\pi(\sigma^2 + \sigma_i^2)) \quad (10)$$

Maximizing the log-likelihood can be performed by searching for μ^* and σ^* such that $\frac{\partial}{\partial \mu} L = 0$ and $\frac{\partial}{\partial \sigma} L = 0$. In the case with no experimental error ($\sigma_i=0$), we find back the well known mean and standard deviation maximum likelihood estimates: $\mu^* = \frac{1}{n} \sum_{i=1}^n x_i$ and $\sigma^* = \frac{1}{n} \sum_{i=1}^n (x_i - \mu^*)^2$.

Searching for μ^* and σ^* numerically, we found a mean estimate of 5.6 ± 4.6 meV/atom and a standard deviation estimate of 24 ± 3.5 meV/atom. The 95% percent confidence intervals have been evaluated using Fischer’s information matrix.⁶⁵ From this normal model of the DFT error, we see that 90% of the errors should lie within ± 40 meV/atom, providing a reasonable order of magnitude for an “error bar” around the oxides reactions energies relevant for phase stability.

Reaction energies involving a change in oxidation states are expected to be more difficult to model using DFT. In our data set, only three reactions (shown in Table III) involve a change in formal oxidation state (as defined in the ICSD). While the data set is too small to draw any strong conclusion, the few reaction energies involving a change in oxidation states do not show larger errors than the typical errors found for the entire data set.

Reaction	Change in Oxidation State	$\Delta E_{\text{GGA}+U}^{\text{comp}} - \Delta E_{\text{OK}}^{\text{exp}}$ (meV/at)
$\frac{2}{3}\text{Fe}_3\text{O}_4 + \frac{1}{3}\text{Mn}_3\text{O}_4 \rightarrow \text{Fe}_2\text{MnO}_4$	$\text{Fe}^{2+}, \text{Mn}^{3+} \rightarrow \text{Fe}^{3+}, \text{Mn}^{2+}$	14
$\frac{1}{2}\text{Fe}_2\text{O}_3 + \frac{1}{2}\text{MoO}_3 + \frac{1}{2}\text{MoO}_2 \rightarrow \text{FeMoO}_4$	$\text{Fe}^{3+}, \text{Mo}^{4+} \rightarrow \text{Fe}^{2+}, \text{Mo}^{6+}$	14
$\frac{1}{2}\text{Mn}_2\text{O}_3 + \frac{1}{2}\text{MoO}_3 + \frac{1}{2}\text{MoO}_2 \rightarrow \text{MnMoO}_4$	$\text{Mn}^{3+}, \text{Mo}^{4+} \rightarrow \text{Mn}^{2+}, \text{Mo}^{6+}$	34

TABLE III: Difference between computed and experimental reaction energies in GGA+ U for reaction energies involving change in formal oxidation states (as defined by the ICSD).

It has been demonstrated that GGA+ U is required to accurately predict the reaction energies of transition metals oxides when a change in oxidation state is involved (redox reactions).^{37,51} As most reaction energies studied in this work do not involve changes in oxidation state, it is of interest to probe if the Hubbard U parameter is beneficial to the accuracy of reaction energies. Therefore, for all reactions involving at least one element requiring a U value (see Methods), we also computed the GGA (without U) reaction energy and compared the distribution of errors in the two data sets (GGA and GGA+ U). Applying the previously presented maximum likelihood estimation for both samples (GGA and GGA+ U), we find the means for both sets to be close to zero (-1.1 ± 21 meV/atom in GGA and -4.6 ± 6.3 meV/atom for GGA+ U) showing no conclusive difference in terms of the mean and therefore in the tendency to overestimate or underestimate reaction energies. On the other hand, the standard deviation is significantly higher for GGA (69 ± 15 meV/atom) than for GGA+ U (19 ± 5.3 meV/atom), indicating significantly larger errors when no Hubbard U parameter is used. Table IV illustrates this result by presenting the compounds with the largest difference between the error with GGA+ U and the error with GGA. Some reactions, such as those forming FeMoO_4 and Fe_2MnO_4 , involve change in formal oxidation states and are, not surprisingly, better represented with

GGA+ U . However, even reaction energies without any change in formal valence (i.e., the reactions forming NaFeO₂, Cr₂FeO₄, Co₂SiO₄, MnTiO₃ and Mn₂TiO₄) show better accuracy in GGA+ U . This is likely due to the fact that all reactions, even those without a formal change in oxidation state, can involve change in bonding and charge transfer. The use of the Hubbard U is therefore necessary to correct for the self-interaction error arising from these charge transfers.

reaction	$\Delta E_{\text{GGA}}^{\text{comp}} - \Delta E_{\text{0K}}^{\text{exp}}$ (meV/at)	$\Delta E_{\text{GGA}+U}^{\text{comp}} - \Delta E_{\text{0K}}^{\text{exp}}$ (meV/at)
$\frac{2}{3}\text{Fe}_3\text{O}_4 + \frac{1}{3}\text{Mn}_3\text{O}_4 \rightarrow \text{Fe}_2\text{MnO}_4$	355	14
$\text{Cr}_2\text{O}_3 + \text{FeO} \rightarrow \text{Cr}_2\text{FeO}_4$	71	-14
$2\text{CoO} + \text{SiO}_2 \rightarrow \text{Co}_2\text{SiO}_4$	64	-12
$\text{MnO} + \text{TiO}_2 \rightarrow \text{MnTiO}_3$	-76	-25
$2\text{MnO} + \text{TiO}_2 \rightarrow \text{Mn}_2\text{TiO}_4$	-88	-10
$\frac{1}{2}\text{Fe}_2\text{O}_3 + \frac{1}{2}\text{MoO}_3 + \frac{1}{2}\text{MoO}_2 \rightarrow \text{FeMoO}_4$	-74	14
$\frac{1}{2}\text{Na}_2\text{O} + \frac{1}{2}\text{Fe}_2\text{O}_3 \rightarrow \text{NaFeO}_2$	-128	-51

TABLE IV: Difference between computed and reaction energies for GGA+ U and GGA. Only the reactions with the largest difference between GGA and GGA+ U results are presented (≥ 50 meV/atom)

In contrast to most previous work comparing experimental thermochemical data with DFT results, we performed a heat capacity integration to make sure we compare DFT results to zero K energies (instead of 298K). When formation energies are calculated from the elements, the DFT error (rms of 200 meV/atom)⁵² is so large that the heat capacity integration is not relevant. However, in our study where the DFT error is smaller it is difficult to *a priori* decide to neglect the heat capacity integration down to zero K. Comparing the error distribution obtained with and without the heat capacity integration, we observe a larger standard deviation when the integrated heat capacity is not taken into account (31 ± 4.2 meV/atom vs 24 ± 3.5 meV/atom). On average, the contribution of the heat capacity integration is smaller than the DFT error (mean absolute component of the heat capacity integration is 12 meV/atom) but for some reactions, its effect can be large enough to be necessary to achieve a good accuracy. We present in Table V a few of the reaction energies with the largest integrated heat capacity components (i.e., the largest $|\Delta E_{298\text{K}}^{\text{exp}} - \Delta E_{\text{0K}}^{\text{exp}}|$). For all those reactions, including the heat capacity component improves the agreement between computations and experiments. Many of those reactions involve aluminum-based compounds because of a large mismatch between the Debye temperature for Al₂O₃ (897K) and for some of the aluminum containing ternaries such as Ba₃Al₂O₆ (308K), Ca₃Al₂O₆ (523 K) and CaAl₄O₇ (593K).

Reaction	$\Delta E_{298\text{K}}^{\text{exp}} - \Delta E_{\text{0K}}^{\text{exp}}$ (meV/at)	$\Delta E_{\text{0K}}^{\text{comp}} - \Delta E_{\text{0K}}^{\text{exp}}$ (meV/at)	$\Delta E_{\text{0K}}^{\text{comp}} - \Delta E_{298\text{K}}^{\text{exp}}$ (meV/at)
$2\text{Na}_2\text{O} + \text{V}_2\text{O}_5 \rightarrow \text{Na}_4\text{V}_2\text{O}_7$	47	3	-45
$\text{K}_2\text{O} + 2\text{B}_2\text{O}_3 \rightarrow \text{K}_2\text{B}_4\text{O}_7$	-45	0	45
$\text{Al}_2\text{O}_3 + 3\text{BaO} \rightarrow \text{Ba}_3\text{Al}_2\text{O}_6$	42	17	-25
$\text{Al}_2\text{O}_3 + 3\text{CaO} \rightarrow \text{Ca}_3\text{Al}_2\text{O}_6$	54	-21	-75
$2\text{Al}_2\text{O}_3 + 3\text{CaO} \rightarrow \text{CaAl}_4\text{O}_7$	52	-42	-93

TABLE V: Comparison between experimental zero K energy (with heat capacity integration) and experimental 298K energy for the compounds with the largest influence of the heat capacity integration on the reaction energy (≥ 40 meV/atom).

IV. DISCUSSION

We have presented a comparison between experimental and DFT energies of reactions across a large set of oxide chemistries and crystal structures. For a dataset of reaction energies relevant to phase stability, the distribution of the error between GGA+ U computations and experiments has been provided. In addition, we analyzed how those errors depend on chemistries and are influenced by the use of a Hubbard U parameter.

While we tried as much as possible to remove unreliable experimental data from our data set, we must stress that our results depend on the quality of the experimental data. Our work already identified a few large discrepancies between the Kubachewski tables and data from NIST (e.g., K_2SiO_3 with a 216 meV/atom difference, and $\text{Mg}_2\text{Ti}_2\text{O}_5$ with a 72 meV/atom difference), or the Landolt-Bornstein database (FeMoO_4 with a 20 meV/atom discrepancy, $\text{Na}_4\text{V}_2\text{O}_7$ with a 88 meV/atom discrepancy, Na_2MoO_4 with a 97 meV/atom discrepancy and KFeO_2 with a 1420 meV/atom error), as well as very likely errors in both of these databases (e.g., $\text{Na}_2\text{Mo}_2\text{O}_7$ and BaMoO_4). Another possible source of error in our data set can come from an inadequate choice of crystal structure among polymorphs as only partial crystallographic information is usually provided in the Kubachewski tables (e.g., $\text{Ca}_3(\text{PO}_4)_2$).

A few computational assumptions also influence our results. Due to the high-throughput nature of our investigation, we only tested specific magnetic states of compounds: FM or AFM. Any magnetic ground state more complex would have been missed. In addition, the U value we used have been fitted on binary oxides formation enthalpies and directly influence the energies obtained. Finally, our results rely on the PAW pseudopotentials used, and would be influenced by any error in their construction or transferability.⁷⁷

The available experimental thermochemical data present some chemical biases influencing our results. While our data covers main group and transition metals well, the rare-earth and transuranides are not as well sampled due to the lack of experimental data available. Future work on those chemistries, relying mainly on extracting more experimental data, would be required to more precisely evaluate the accuracy of their reaction energies.

The most straightforward use of our result is in error detection. By combining DFT computations with our error distribution, we can test the accuracy of uncertain experimental data. For instance, during our experimental data cross-checking process (see Methods section), we identified seven compounds (NaVO_3 , SrB_4O_7 , LiTaO_3 , LiNbO_3 , LaPO_4 , LiB_3O_5 and CdTiO_3) for which the enthalpy provided by the Kubachewski database could not be confirmed by other reliable sources and that we had to exclude from our data set. Among those seven compounds, we find three compounds whose computed formation reaction energies differs from the reported experimental value by a large enough extent to cast major doubt on the Kubachewski data (NaVO_3 by 87 meV/at, CdTiO_3 by 89 meV/atom and LiNbO_3 by 106 meV/atom).

Another critical application of our results lies in the assessment of the accuracy of zero K phase diagrams built from GGA+ U computations. These phase diagrams are useful when studying the phase stability of known but also predicted compounds. Several recent studies relied on such phase diagrams to investigate the stability of new proposed phosphates-based compounds for lithium-ion batteries,²⁰⁻²² new predicted ternary oxides,¹⁸ new iron borides¹⁷ or new intermetallics.^{16,26} Zero K phase diagrams based on GGA computations for all compounds in the ICSD are also available online through the *Materials Project*.^{40,66}

Zero K phase diagrams are typically built using the convex hull construction, which effectively evaluates the stability for a given compound against any linear combination of compounds that has the same composition. From this construction, there is one critical reaction energy that will ultimately determine if a compound is stable (on the convex hull) or not (see Methods section). It is very common for those critical reactions to involve only very chemically similar compounds when multi-component systems are studied. For instance, we show in Figure 5.a the Li-Al-O phase diagram constructed from the calculated energy of the relevant phases in the ICSD. The black arrows indicate what phases will be involved in the reaction critical to phase stability. For the two ternary oxides, LiAlO_2 and Li_5AlO_4 , the reaction energies determining their stability are respectively: $\frac{1}{5}\text{Li}_5\text{AlO}_4 + \frac{2}{5}\text{Al}_2\text{O}_3 \rightarrow \text{LiAlO}_2$ and $2\text{Li}_2\text{O} + \text{LiAlO}_2 \rightarrow \text{Li}_5\text{AlO}_4$. The relevant reaction energies involve oxides (i.e., chemically similar compounds) and, while there are metallic elements (Li, and Al) and intermetallics (LiAl , Li_3Al , Li_3Al_2) present in the phase diagram, those are not directly involved in determining whether the ternary oxides are stable or not. Figure 5.b shows the Li-Cr-O phase diagram which is more complicated due to the large number of oxidation states that Cr can form (+3 to +6). For LiCrO_2 , the reaction determining phase stability is $\frac{1}{2}\text{Cr}_2\text{O}_3 + \frac{1}{2}\text{Li}_2\text{O} \rightarrow \text{LiCrO}_2$. Again, this reaction involves only Cr^{3+} -based oxides. The reaction energies with respect to the elements or chromium phases at other oxidation states (e.g., CrO_2 , CrO_3 , and Li_2CrO_4) do not directly influence the stability of LiCrO_2 . Similarly, the stability of Li_2CrO_4 depends directly on reaction energies with respect with Li_2O and another Cr^{6+} oxide: CrO_3 . On the other hand, Li_3CrO_4 depends on a more complicated reaction involving Li_2CrO_4 , LiCrO_2 and Li_2O . This reaction still does not involve metallic elemental phases but is a redox reaction (involving Cr in +3 and +6 states).

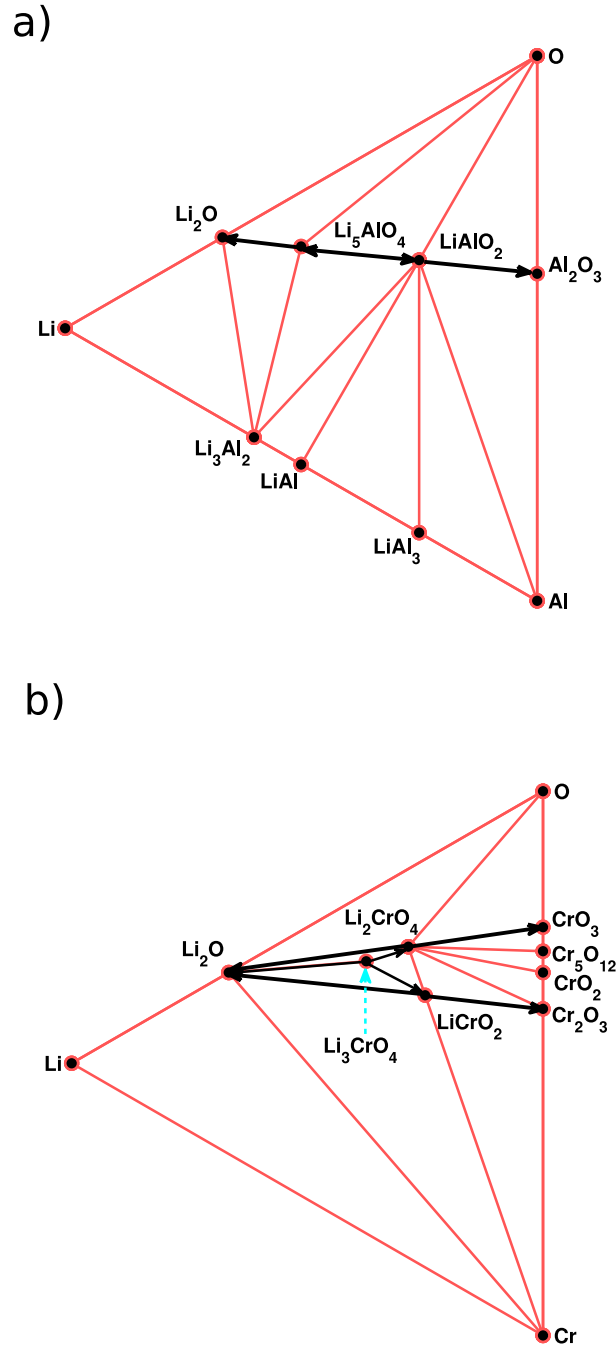


FIG. 5: (Color Online) Two examples of ternary oxides zero K phase diagrams: Li-Al-O (a) and Li-Cr-O (b). All phases are from the ICSD. We excluded phases with partial occupancies. The Li-Al-O phase diagram illustrates the case of elements with only one oxidation state. On the other hand Cr in the Li-Cr-O phase diagram is common in oxidation states from +3 to +6. The black (dark gray) arrows indicate the critical reaction energies determining the stability of ternary phases. The light blue (gray) dashed arrow indicates the Li_3CrO_4 phase.

The situation we illustrated with the Li-Al-O and Li-Cr-O phase diagram is very common. For all ternary oxides present in the ICSD database, 80% compete for phase stability through reactions involving only oxides reactions with no change in formal oxidation state. In those common cases, the DFT error distribution we found in our work can be used to assess the accuracy of zero K GGA+ U phase diagrams. For instance, when a new compound is proposed its energy for decomposition to other stable phases can be computed through the convex hull constructions. Using the DFT error distribution, we can take into account inherent errors within DFT and evaluate the likelihood for a DFT

error to result in incorrectly predicting the stability of a compound. For example, a compound computed to be 50 meV/atom above the convex hull (i.e., having a decomposition energy to other phases around 50 meV/atom) is likely to actually be unstable at zero K as such a large error would be two standard deviation away from the mean. Similarly, when a predicted compound is stable versus competing phases (i.e., on the convex hull), our error distribution can be used to assess the probability that its stability is due to a DFT error. We should note that, while not common, there are instances where the reaction energy critical to phase stability involves compounds very different chemically (e.g., a ternary oxide competing versus a metal or versus phases with different oxidation states). In those cases, caution must be exerted in the interpretation of the results, and it is possible that the typical errors can be larger than the ones presented in this work. While our study did not show any large discrepancy for reaction energies involving oxides with different oxidation states, our data set (three reactions) was too limited to derive strong conclusions. On the other hand, it is extremely likely that the errors on reaction energies involving oxides and metallic phases will be much higher than the errors obtained in this work. Indeed, solid elemental phases are often metallic and formation energies from the elements for ternary oxides show much larger errors due to smaller cancellation of errors.^{51,52,67}

By noting that most reactions relevant for phase stability involve chemically similar compounds and providing an error distribution for those reactions, our work also removes an apparent paradox on the accuracy of zero K phase diagram. DFT-calculated zero K phase diagrams are often quite accurate in predicting the correct stable phases. The Li-Fe-P-O phase diagram presented in Ong et al.¹⁰ for instance shows very good agreement with experimental phase stability. This success is surprising when compared with the magnitude of the reported errors in DFT elemental formation energies (rms of 240 meV/atom).⁵² Our work resolves this apparent contradiction by noting that reaction energies from the elements are in general not relevant to phase stability and that the error distribution is much smaller for the reaction energies relevant to phase stability.

Interestingly, our work shows that, when transition metals with partially occupied *d*-shell are involved, the accuracy of DFT is significantly lower for GGA than for GGA+*U* even for reaction energies involving no change in formal oxidation state. Unfortunately, GGA+*U* is known to fail at modeling metallic and intermetallic phases, leading to larger errors in the regions of the phase diagram involving those phases. Our results reinforce the need to use either higher level theories or schemes to mix GGA and GGA+*U* such as the one developed by Jain et al.⁶⁷ to obtain accurate phase diagrams that cover chemically diverse regions of composition space.

This work only focused on oxides due to the lack of thermochemical data in other types of ternary semiconducting or insulating materials (e.g., halides or sulfides). However, we believe that the conclusions might be of more general character. The very limited set of fluorides present in the Kubachewski tables (Li_2BeF_4 , Li_3AlF_6 and Na_3AlF_6) show errors for reaction energies from binary to ternary fluorides of respectively -20 meV/atom, -6 meV/atom and 6 meV/atom which are within the error distribution found for oxides. We should however warn the reader that our data did not include any peroxides (i.e., oxides containing oxygen-oxygen bonds as O_2^{2-}) and we have experienced that peroxides tend to be overstabilized in GGA due to the overbinding of the O-O bond (similarly to the overbinding of the oxygen molecule).⁶⁸ While peroxides are rare, other chemistries such as sulfides or nitrides tend to form those type of covalent bonds more easily in solids (e.g., persulfides, or pernitrides) and might suffer more often from this possible error.

We hope the work presented in this paper will motivate future thermochemical evaluation of alternative functionals. It would be for instance of interest to compare the performances of new functionals, such as AM05 and HSE,⁶⁹⁻⁷² or more advanced techniques, such as Quantum Monte-Carlo,⁷³ to GGA+*U*. While bulk modulus and lattice constants are often tested when new methods or functionals are proposed, it is rare to evaluate the accuracy of reaction energies. We hope the material provided in this work can constitute a standard data set to perform future benchmarks.

V. CONCLUSION

We have estimated the error in GGA+*U* in reproducing reaction energies relevant to phase stability in ternary oxides. This error is distributed normally with a mean close to zero and a standard deviation of 24 meV/atom. The errors we found are much smaller than the error on the more commonly reported reaction energies from the elements. We attribute this to the larger cancellation of errors involved in reaction energies among chemically similar compounds. Our results can be used to assess the accuracy of zero K phase diagrams as the relevant reaction energies when building phase diagrams involve chemically similar compounds. Finally, our analysis also demonstrates the importance of using a Hubbard *U* parameter to model reaction energies involving transition metals even when no change in formal oxidation states is occurring.

VI. ACKNOWLEDGMENTS

The authors would like to acknowledge Chris Fischer and Tim Mueller for helpful discussion. This work was supported by the NSF (under Contract No. DMR-0606276) and by the Department of Energy, Office of Basic Energy Sciences (under Contract No DE-FG02-96ER4557). Anubhav Jain would like to acknowledge funding from the U.S. Department of Energy through the Department of Energy Computational Science Graduate Fellowship (DOE CSGF) (under Grant No. DE-FG02-97ER25308).

Appendix A

The table below gives the VASP pseudopotentials used in this work and the value of the Hubbard U (if any) on each element.

Element	VASP PAW pseudopotential	U (eV)	Element	VASP PAW pseudopotential	U (eV)
Ag	Ag 06Sep2000	1.5	Li	Li 17Jan2003	/
Al	Al 04Jan2001	/	Mg	Mg 05Jan2001	/
Ba	Ba_sv 06Sep2000	/	Mn	Mn 06Sep2000	3.9
B	B 06Sep2000	/	Mo	Mo_pv 08Apr2002	4.38
Be	Be 06Sep2000	/	Na	Na 08Apr2002	/
Ca	Ca_sv 06Sep2000	/	Nb	Nb_pv 08Apr2002	1.5
Cd	Cd 06Sep2000	/	Ni	Ni 06Sep2000	6.0
Ce	Ce 28Sep2000	/	O	O 08Apr2002	/
Co	Co 06Sep2000	3.4	Pb	Pb 08Apr2002	/
Cr	Cr 06Sep2000	3.5	P	P 17Jan2003	/
Cs	Cs_sv 08Apr2002	/	Rb	Rb_pv 06Sep2000	/
Cu	Cu 05Jan2001	4.0	Se	Se 06Sep2000	/
Fe	Fe 06Sep2000	4.0	Si	Si 05Jan2001	/
Ge	Ge 05Jan2001	/	Sr	Sr_sv 07Sep2000	/
Hf	Hf 20Jan2003	/	Ti	Ti 08Apr2002	/
Hg	Hg 06Sep2000	/	U	U 06Sep2000	/
K	K_sv 06Sep2000	/	V	V_pv 07Sep2000	3.1
La	La 06Sep2000	/	Zn	Zn 06Sep2000	/
			Zr	Zr 08Apr2002	/

Appendix B

Heat capacity data down to zero K is not available for all compounds used in our work. To obtain the enthalpy at zero K from the provided enthalpies at 298K, we estimated the heat capacity at low temperature by a fitting procedure (see Methods). We used the experimental heat capacity and entropy at 298K to fit a Debye-like model. This model was then integrated down to zero K and subtracted from the enthalpy at 298K to provide the enthalpy at zero K. In this section, we will compare, for a few compounds which have experimentally known heat capacity data, the results of our fitting procedure to the direct heat capacity measurement.

Figure 6 shows the heat capacity vs temperature curve fitted to the Debye-like model (red line) and experimentally determined for a few compounds: MgO,⁷⁴ BaO,⁷⁴ ZnO,⁷⁴ Cs₂O,⁷⁵ FeO,⁷⁶ and CoFe₂O₄.⁴⁷ A very good agreement between both data sets can be observed for all compounds, validating our approach.

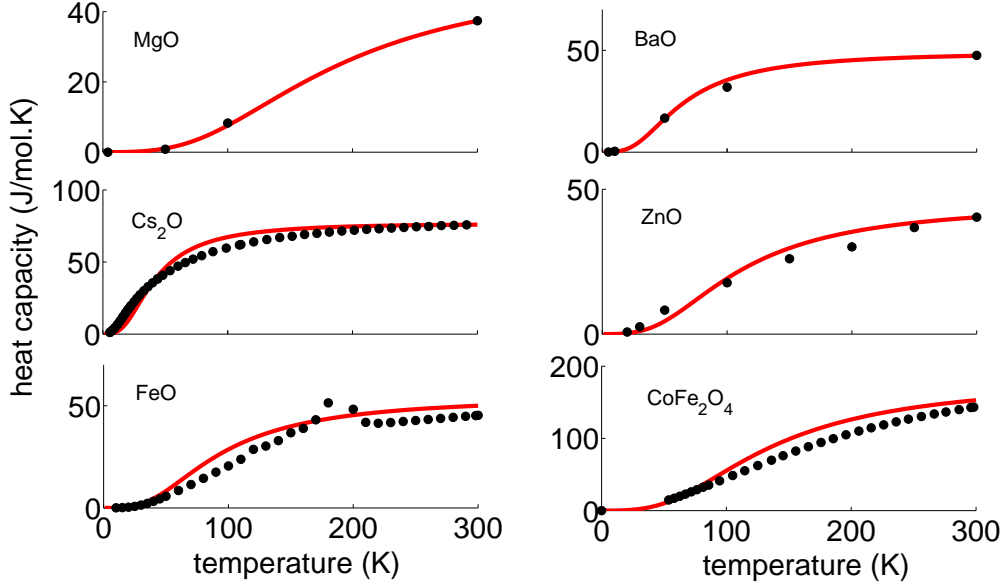


FIG. 6: (Color Online) Heat capacity vs temperature for several compounds (MgO, BaO, ZnO, Cs₂O, FeO, and CoFe₂O₄). The black dots are experimental values and the red line is the fitted Debye-like model. All heat capacities are given in J/mol-fu.K.

Table VI shows the difference between the integrated heat capacity from zero K to 298K from our fitted model and obtained directly from experiments. The good agreement in terms of heat capacity vs temperature curves is reflected into the small difference between the integrated heat capacity (from 2 to 5 meV/atom).

formula	Integrated Heat Capacity from Direct Exp. (meV/at)	Integrated Heat Capacity from fitted Debye Model (meV/at)	Difference (meV/at)
MgO	24.9	26.6	1.7
BaO	49.2	53.6	4.4
Cs ₂ O	61.9	63.9	2.0
ZnO	35.6	37.7	2.1
FeO	45.4	50.1	4.7
CoFe ₂ O ₄	32.6	37.2	4.6

TABLE VI: Integrated heat capacity from zero K to 298K. Values obtained directly from experiments and through the fitted Debye model.

Our approach was not aimed at reproducing very accurately the Debye temperature but we compared our fitted Debye temperature to non-calorimetric-based Debye temperature measurements when present in the Landolt-Bornstein database. From neutron scattering experiments on MgO, the Debye temperature is reported to be 743K and our fitted value is 779K. From elastic constant measurements, we find 291K for BaO, 416K for ZnO and 494K for FeO which compares well with 266K, 455K and 383K respectively found from our fit.

Appendix C

The table below gives the ICSD number of the corresponding crystal structure, the experimental formation energy from the element (given at zero K through heat capacity integration), the experimental error on the formation enthalpy from the element, the computed total energy (in GGA and GGA+*U*) and the source of the experimental data.

formula	ICSD number	Exp. formation enthalpy (eV/at)	Exp. error (eV/at)	Computed total energy GGA+ <i>U</i> (eV/at)	Computed total energy GGA (eV/at)	source
Ag ₂ CrO ₄	16298	-1.114	0.011	-5.265	-6.045	Kuba

Ag ₂ O	35540	-0.162	0.002	-3.195	-3.63	Kuba
AlCeO ₃	72558	-3.767	0.006	-8.08	-8.08	Kuba
AlLaO ₃	92523	-3.75	0.007	-8.015	-8.015	Kuba
AlLiO ₂	28288	-3.106	0.011	-6.614	-6.614	Kuba
AlNaO ₂	79404	-2.968	0.011	-6.351	-6.351	NIST
AlPO ₄	72374	-3.021	0.004	-7.476	-7.476	Kuba
Al ₂ BaO ₄	75426	-3.475	0.012	-7.226	-7.226	Kuba
Al ₂ Ba ₃ O ₆	79558	-3.348	0.012	-6.79	-6.79	Kuba
Al ₂ BeO ₄	31080	-3.427	0.009	-7.394	-7.394	Kuba
Al ₂ CaO ₄	260	-3.473	0.003	-7.245	-7.245	Kuba
Al ₂ Ca ₃ O ₆	1841	-3.416	0.004	-6.947	-6.947	Kuba
Al ₂ FeO ₄	56117	-2.94	0.004	-7.34	-7.504	Kuba
Al ₂ MgO ₄	29444	-3.431	0.011	-7.11	-7.11	NIST
Al ₂ O ₃	43732	-3.494	0.003	-7.481	-7.481	Kuba
Al ₂ SrO ₄	26466	-3.492	0.025	-7.205	-7.205	Kuba
Al ₂ ZnO ₄	94158	-3.091	0.004	-6.706	-6.706	Kuba
Al ₂ SiO ₅	28272	-3.384	0.011	-7.633	-7.633	NIST
Al ₂ TiO ₅	24133	-3.404	0.022	-7.976	-7.976	Kuba
Al ₄ CaO ₇	34487	-3.481	0.003	-7.364	-7.364	Kuba
Al ₆ BeO ₁₀	95408	-3.45	0.006	-7.444	-7.444	Kuba
BCsO ₂	74888	-2.57	0.054	-6.626	-6.626	Kuba
BKO ₂	16005	-2.611	0.022	-6.725	-6.725	Kuba
BLiO ₂	16568	-2.665	0.004	-7.017	-7.017	Kuba
BNaO ₂	34645	-2.559	0.006	-6.759	-6.759	Kuba
BRbO ₂	59826	-2.564	0.054	-6.649	-6.649	Kuba
B ₂ CaO ₄	20097	-3.028	0.006	-7.756	-7.756	Kuba
B ₂ Ca ₂ O ₅	280076	-3.165	0.006	-7.532	-7.532	Kuba
B ₂ Ca ₃ O ₆	23664	-3.257	0.004	-7.372	-7.372	Kuba
B ₂ O ₃	24047	-2.66	0.004	-8.023	-8.023	Kuba
B ₃ NaO ₅	2045	-2.671	0.008	-7.532	-7.532	Kuba
B ₄ CaO ₇	200081	-2.907	0.005	-7.902	-7.902	Kuba
B ₄ K ₂ O ₇	2833	-2.683	0.011	-7.292	-7.292	NIST
B ₄ Li ₂ O ₇	300010	-2.704	0.011	-7.445	-7.445	NIST
B ₄ Na ₂ O ₇	2040	-2.638	0.011	-7.304	-7.304	NIST
B ₈ Na ₂ O ₁₃	14355	-2.682	0.005	-7.654	-7.654	Kuba
BaMoO ₄	50821	-2.659	0.012	-7.088	-7.954	Kuba
BaO	52278	-2.894	0.011	-5.913	-5.913	Kuba
BaSiO ₃	6245	-3.389	0.015	-7.405	-7.405	Kuba
BaTiO ₃	31155	-3.453	0.024	-7.935	-7.935	Kuba
BaZrO ₃	97462	-3.709	0.012	-8.296	-8.296	Kuba
BaUO ₄	36239	-3.483	0.004	-8.705	-8.705	Kuba
Ba ₂ SiO ₄	6246	-3.405	0.006	-7.119	-7.119	Kuba
Ba ₂ TiO ₄	2625	-3.351	0.019	-7.45	-7.45	Kuba
BeO	29271	-3.173	0.017	-7.11	-7.11	Kuba
Be ₂ SiO ₄	85484	-3.155	0.011	-7.459	-7.459	NIST
CaCr ₂ O ₄	6131	-2.743	0.011	-7.542	-8.144	Kuba
CaFe ₂ O ₄	28177	-2.228	0.011	-6.756	-7.247	Kuba
CaGeO ₃	403086	-2.697	0.011	-6.558	-6.558	Kuba
CaMoO ₄	409785	-2.706	0.006	-7.087	-7.951	Kuba
CaNb ₂ O ₆	15208	-3.116	0.02	-8.223	-8.551	Kuba
CaO	52783	-3.325	0.004	-6.439	-6.439	Kuba
CaSiO ₃	201538	-3.419	0.004	-7.49	-7.49	Kuba
CaTiO ₃	94568	-3.476	0.01	-8.016	-8.016	Kuba
CaZrO ₃	37264	-3.696	0.02	-8.345	-8.345	Kuba
CaUO ₄	31631	-3.488	0.007	-8.747	-8.747	Kuba
CaV ₂ O ₆	21064	-2.717	0.006	-7.43	-8.14	Kuba
Ca ₂ Fe ₂ O ₅	88989	-2.495	0.006	-6.686	-7.143	Kuba
Ca ₂ SiO ₄	9095	-3.479	0.008	-7.259	-7.259	Kuba
Ca ₂ P ₂ O ₇	22225	-3.174	0.02	-7.27	-7.27	Kuba
Ca ₂ V ₂ O ₇	20609	-2.94	0.006	-7.352	-7.942	Kuba
Ca ₃ Si ₅ O ₇	34354	-3.437	0.011	-7.352	-7.352	Kuba
Ca ₃ P ₂ O ₈	200202	-3.314	0.02	-7.243	-7.243	Kuba
Ca ₃ V ₂ O ₈	412273	-3.048	0.007	-7.218	-7.73	Kuba
Ca ₄ Ti ₃ O ₁₀	86242	-3.493	0.011	-7.828	-7.828	Kuba
CdO	24802	-1.384	0.004	-3.956	-3.956	Kuba
CdSeO ₃	75274	-1.237	0.011	-4.851	-4.851	Kuba
CeCrO ₃	4115	-3.216	0.024	-8.329	-8.643	Kuba
Ce ₂ O ₃	96202	-3.778	0.003	-8.687	-8.687	Kuba
CoCr ₂ O ₄	61612	-2.155	0.01	-7.436	-8.194	Kuba
CoO	17013	-1.279	0.003	-5.62	-6.656	Kuba
CoSeO ₃	80401	-1.238	0.022	-5.636	-5.824	Kuba
CoTiO ₃	48107	-2.539	0.008	-7.756	-7.976	Kuba
Co ₂ SiO ₄	65751	-2.109	0.007	-6.856	-7.145	Kuba
CrCs ₂ O ₄	30204	-2.164	0.005	-5.828	-6.443	Kuba
CrK ₂ O ₄	2402	-2.103	0.006	-5.887	-6.495	Kuba
CrNaO ₂	24595	-2.308	0.012	-6.606	-7.101	Kuba
CrNa ₂ O ₄	26330	-2.017	0.014	-5.892	-6.503	Kuba
CrO ₃	38125	-1.554	0.028	-6.565	-7.624	Kuba
Cr ₂ CuO ₄	16708	-1.95	0.011	-6.864	-7.679	Kuba
Cr ₂ FeO ₄	43269	-2.178	0.007	-7.657	-8.383	Kuba
Cr ₂ MgO ₄	97202	-2.661	0.005	-7.415	-7.993	Kuba
Cr ₂ NiO ₄	28835	-2.071	0.006	-6.879	-7.938	Kuba
Cr ₂ O ₃	107035	-2.384	0.016	-7.888	-8.739	Kuba
Cr ₂ ZnO ₄	24495	-2.324	0.007	-7.012	-7.575	Kuba
Cs ₂ MoO ₄	9278	-2.293	0.011	-5.94	-6.697	Kuba
Cs ₂ O	27919	-1.259	0.01	-3.2	-3.2	Kuba
Cs ₂ UO ₄	20581	-2.905	0.007	-7.321	-7.321	Kuba

CuO	67850	-0.846	0.011	-4.272	-4.917	NIST
FeKO ₂	94467	-1.83	0.011	-5.794	-6.21	Kuba
FeMoO ₄	43013	-1.889	0.011	-7.069	-8.136	Lando
FeNaO ₂	33763	-1.848	0.015	-5.882	-6.444	Kuba
FeO	76639	-1.46	0.036	-6.515	-7.539	Kuba
FeTiO ₃	9805	-2.602	0.012	-8.073	-8.363	Kuba
Fe ₂ MnO ₄	24497	-1.858	0.007	-7.126	-7.545	Kuba
Fe ₂ O ₃	41541	-1.74	0.007	-6.781	-7.511	Kuba
Fe ₂ SiO ₄	34817	-2.214	0.012	-7.36	-7.66	Kuba
Fe ₂ ZnO ₄	91827	-1.779	0.009	-6.221	-6.618	Kuba
Fe ₃ O ₄	31157	-1.697	0.011	-6.805	-7.633	NIST
GeMgO ₃	35534	-2.532	0.01	-6.291	-6.291	Kuba
GeO ₂	92551	-2.029	0.005	-6.39	-6.39	Kuba
HfO ₂	27313	-3.896	0.006	-10.189	-10.189	Kuba
HfSrO ₃	86830	-3.736	0.025	-8.704	-8.704	Kuba
HgO	14124	-0.522	0.004	-2.914	-2.914	Kuba
HgSeO ₃	412547	-0.804	0.011	-4.357	-4.357	Kuba
K ₂ O	60438	-1.311	0.01	-3.409	-3.409	Kuba
K ₂ SiO ₃	201163	-2.712	0.011	-6.078	-6.078	NIST
K ₂ Si ₂ O ₅	52156	-2.924	0.01	-6.723	-6.723	Kuba
K ₂ Si ₄ O ₉	2155	-3.015	0.01	-7.217	-7.217	Kuba
La ₂ O ₃	96201	-3.763	0.006	-8.405	-8.405	Kuba
LiPO ₃	85714	-2.628	0.008	-6.725	-6.725	Kuba
Li ₂ O	57411	-2.091	0.003	-4.771	-4.771	Kuba
Li ₂ SiO ₃	16626	-2.873	0.018	-6.563	-6.563	Kuba
Li ₂ TiO ₃	15150	-2.913	0.018	-7.008	-7.008	Kuba
Li ₂ ZrO ₃	31941	-3.073	0.012	-7.243	-7.243	Kuba
MgMoO ₄	20418	-2.453	0.009	-6.79	-7.658	Kuba
MgO	52026	-3.144	0.002	-5.983	-5.983	Kuba
MgSiO ₃	30893	-3.236	0.008	-7.189	-7.189	Kuba
MgTiO ₃	55285	-3.288	0.004	-7.743	-7.743	Kuba
MgUO ₄	24725	-3.243	0.005	-8.443	-8.443	Kuba
MgTi ₂ O ₅	37232	-3.283	0.011	-8.159	-8.159	NIST
MgV ₂ O ₆	10391	-2.566	0.006	-7.21	-7.921	Kuba
Mg ₂ SiO ₄	88023	-3.249	0.004	-6.885	-6.885	Kuba
Mg ₂ V ₂ O ₇	93603	-2.703	0.008	-7.048	-7.645	Kuba
Mg ₃ P ₂ O ₈	31005	-3.014	0.011	-6.886	-6.886	NIST
MnMoO ₄	15615	-2.097	0.017	-7.409	-8.444	Kuba
MnO	53928	-2.042	0.007	-7.764	-8.238	Kuba
MnSiO ₃	34160	-2.772	0.005	-7.903	-8.087	Kuba
MnTiO ₃	60006	-2.854	0.011	-8.481	-8.715	Kuba
Mn ₂ O ₃	9090	-2.025	0.004	-7.501	-8.235	Kuba
Mn ₂ SiO ₄	26376	-2.601	0.006	-7.904	-8.176	Kuba
Mn ₂ TiO ₄	22313	-2.632	0.011	-8.283	-8.622	Kuba
Mn ₃ O ₄	76088	-2.092	0.003	-7.627	-8.345	Kuba
MoNa ₂ O ₄	44523	-2.214	0.011	-6.082	-6.825	Lando
MoO ₂	36263	-2.06	0.006	-7.618	-8.802	Kuba
MoO ₃	76365	-1.965	0.002	-6.99	-8.256	Kuba
MoPbO ₄	39137	-1.862	0.009	-6.623	-7.481	Kuba
MoSrO ₄	23700	-2.713	0.017	-7.061	-7.925	Kuba
Mo ₂ Na ₂ O ₇	24312	-2.263	0.012	-6.461	-7.392	Kuba
NaPO ₃	18139	-2.562	0.004	-6.556	-6.556	Kuba
Na ₂ O	60435	-1.486	0.011	-3.781	-3.781	NIST
Na ₂ SiO ₃	24664	-2.734	0.011	-6.201	-6.201	Kuba
Na ₂ UO ₄	79423	-2.838	0.004	-7.47	-7.47	Kuba
Na ₂ Si ₂ O ₅	34688	-2.88	0.006	-6.785	-6.785	Kuba
Na ₂ Ti ₃ O ₇	15463	-3.042	0.004	-7.749	-7.749	Kuba
Na ₃ PO ₄	97205	-2.52	0.003	-5.851	-5.851	Kuba
Na ₄ SiO ₄	15500	-2.458	0.029	-5.509	-5.509	Kuba
Na ₄ P ₂ O ₇	10370	-2.56	0.011	-6.165	-6.165	Kuba
Na ₄ V ₂ O ₇	35635	-2.374	0.011	-6.204	-6.708	Lando
Nb ₂ O ₅	25750	-2.847	0.006	-8.583	-8.96	Kuba
NiO	24018	-1.278	0.007	-5.059	-5.748	Kuba
NiSeO ₃	416251	-1.212	0.011	-5.221	-5.493	Kuba
NiTiO ₃	15988	-2.523	0.013	-7.349	-7.654	Kuba
Ni ₂ SiO ₄	202376	-2.103	0.014	-6.313	-6.714	Kuba
PbO	94333	-1.187	0.004	-5.426	-5.426	Kuba
Rb ₂ O	77676	-1.23	0.029	-3.159	-3.159	Kuba
SrO	28904	-3.113	0.02	-6.052	-6.052	Kuba
ZnO	31060	-1.854	0.003	-4.549	-4.549	Kuba
SeO ₂	24022	-0.815	0.007	-5.151	-5.151	Kuba
SiO ₂	98629	-3.172	0.006	-7.904	-7.904	Kuba
TiO ₂	69331	-3.292	0.003	-8.804	-8.804	Kuba
ZrO ₂	68782	-3.823	0.011	-9.517	-9.517	NIST
PbSeO ₃	1271	-1.159	0.011	-5.438	-5.438	Kuba
PbSiO ₃	26812	-2.408	0.011	-6.968	-6.968	NIST
PbTiO ₃	27949	-2.515	0.029	-7.488	-7.488	Kuba
SeZnO ₃	61341	-1.387	0.008	-5.003	-5.003	Kuba
SiSrO ₃	38271	-3.419	0.008	-7.42	-7.42	Kuba
SrTiO ₃	56718	-3.5	0.016	-7.947	-7.947	Kuba
SrZrO ₃	89354	-3.701	0.03	-8.273	-8.273	Kuba
UO ₃	26673	-3.212	0.003	-9.628	-9.628	Kuba
Pb ₂ SiO ₄	26343	-2.079	0.011	-6.525	-6.525	NIST
SiSr ₂ O ₄	36041	-3.446	0.005	-7.114	-7.114	Kuba
SiZn ₂ O ₄	2425	-2.465	0.005	-6.015	-6.015	Kuba
SiZrO ₄	31130	-3.524	0.011	-8.73	-8.73	NIST

Sr ₂ TiO ₄	20293	-3.426	0.014	-7.436	-7.436	Kuba
P ₂ O ₅	40865	-2.257	0.011	-7.011	-7.011	Kuba
V ₂ O ₅	41030	-2.328	0.003	-7.479	-8.385	Kuba

Appendix D

The table below give all reactions considered in our data set with their associated experimental and computed reaction energies at zero K.

reaction	Computed Reaction Energy GGA+U (eV/at)	Exp. Reaction Energy (eV/at)	Difference (eV/at)
CaO+MoO ₃ → CaMoO ₄	-0.281	-0.288	0.007
TiO ₂ +PbO → PbTiO ₃	-0.036	-0.065	0.029
PbO+SiO ₂ → PbSiO ₃	-0.055	-0.029	-0.025
SeO ₂ +PbO → PbSeO ₃	-0.177	-0.195	0.018
PbO+MoO ₃ → MoPbO ₄	-0.154	-0.156	0.002
2PbO+SiO ₂ → Pb ₂ SiO ₄	-0.037	-0.041	0.003
TiO ₂ +NiO → NiTiO ₃	-0.035	-0.037	0.001
NiO+SeO ₂ → NiSeO ₃	-0.099	-0.212	0.113
NiO+Cr ₂ O ₃ → Cr ₂ NiO ₄	-0.005	-0.004	-0.002
SiO ₂ +2NiO → Ni ₂ SiO ₄	-0.024	-0.014	-0.010
0.5Na ₂ O+0.5P ₂ O ₅ → NaPO ₃	-0.514	-0.536	0.022
0.5Fe ₂ O ₃ +0.5Na ₂ O → FeNaO ₂	-0.255	-0.203	-0.051
0.5Cr ₂ O ₃ +0.5Na ₂ O → CrNaO ₂	-0.256	-0.261	0.005
0.5B ₂ O ₃ +0.5Na ₂ O → BNaO ₂	-0.327	-0.340	0.013
0.5Na ₂ O+1.5B ₂ O ₃ → B ₃ NaO ₅	-0.216	-0.207	-0.010
0.5Al ₂ O ₃ +0.5Na ₂ O → AlNaO ₂	-0.258	-0.227	-0.031
2Na ₂ O+V ₂ O ₅ → Na ₄ V ₂ O ₇	-0.432	-0.434	0.003
2Na ₂ O+SiO ₂ → Na ₄ SiO ₄	-0.354	-0.409	0.056
P ₂ O ₅ +2Na ₂ O → Na ₄ P ₂ O ₇	-0.645	-0.659	0.014
0.5P ₂ O ₅ +1.5Na ₂ O → Na ₃ PO ₄	-0.658	-0.697	0.039
Na ₂ O+UO ₃ → Na ₂ UO ₄	-0.348	-0.366	0.017
3TiO ₂ +Na ₂ O → Na ₂ Ti ₃ O ₇	-0.201	-0.201	0.000
Na ₂ O+SiO ₂ → Na ₂ SiO ₃	-0.359	-0.404	0.046
2SiO ₂ +Na ₂ O → Na ₂ Si ₂ O ₅	-0.256	-0.270	0.015
Na ₂ O+MoO ₃ → MoNa ₂ O ₄	-0.468	-0.454	-0.014
Na ₂ O+2MoO ₃ → Mo ₂ Na ₂ O ₇	-0.346	-0.428	0.082
Na ₂ O+CrO ₃ → CrNa ₂ O ₄	-0.520	-0.492	-0.029
4B ₂ O ₃ +Na ₂ O → B ₈ Na ₂ O ₁₃	-0.184	-0.175	-0.009
Na ₂ O+2B ₂ O ₃ → B ₄ Na ₂ O ₇	-0.260	-0.249	-0.011
TiO ₂ +MnO → MnTiO ₃	-0.086	-0.062	-0.025
SiO ₂ +MnO → MnSiO ₃	-0.042	-0.052	0.010
0.5MoO ₂ +0.5MoO ₃ +0.5Mn ₂ O ₃ → MnMoO ₄	-0.049	-0.084	0.034
0.67Fe ₃ O ₄ +0.33Mn ₃ O ₄ → Fe ₂ MnO ₄	-0.016	-0.029	0.014
2MnO+TiO ₂ → Mn ₂ TiO ₄	-0.064	-0.054	-0.010
SiO ₂ +2MnO → Mn ₂ SiO ₄	-0.067	-0.074	0.007
V ₂ O ₅ +MgO → MgV ₂ O ₆	-0.064	-0.056	-0.007
UO ₃ +MgO → MgUO ₄	-0.030	-0.054	0.024
MgO+TiO ₂ → MgTiO ₃	-0.068	-0.055	-0.013
MgO+2TiO ₂ → MgTi ₂ O ₅	-0.061	-0.027	-0.033
SiO ₂ +MgO → MgSiO ₃	-0.053	-0.075	0.022
MoO ₃ +MgO → MgMoO ₄	-0.136	-0.095	-0.040
GeO ₂ +MgO → GeMgO ₃	-0.063	-0.057	-0.007
MgO+Cr ₂ O ₃ → Cr ₂ MgO ₄	-0.071	-0.060	-0.011
Al ₂ O ₃ +MgO → Al ₂ MgO ₄	-0.057	-0.036	-0.021
3MgO+P ₂ O ₅ → Mg ₃ P ₂ O ₈	-0.350	-0.347	-0.003
2MgO+V ₂ O ₅ → Mg ₂ V ₂ O ₇	-0.113	-0.078	-0.035
2MgO+SiO ₂ → Mg ₂ SiO ₄	-0.079	-0.093	0.014
0.5P ₂ O ₅ +0.5Li ₂ O → LiPO ₃	-0.386	-0.422	0.035
0.5Li ₂ O+0.5B ₂ O ₃ → BLiO ₂	-0.213	-0.219	0.005
0.5Al ₂ O ₃ +0.5Li ₂ O → AlLiO ₂	-0.149	-0.138	-0.011
Li ₂ O+ZrO ₂ → Li ₂ ZrO ₃	-0.099	-0.116	0.017
TiO ₂ +Li ₂ O → Li ₂ TiO ₃	-0.221	-0.222	0.001
Li ₂ O+SiO ₂ → Li ₂ SiO ₃	-0.225	-0.242	0.017
Li ₂ O+2B ₂ O ₃ → B ₄ Li ₂ O ₇	-0.172	-0.175	0.003
0.5La ₂ O ₃ +0.5P ₂ O ₅ → LaPO ₄	-0.473	-0.579	0.106
0.5Al ₂ O ₃ +0.5La ₂ O ₃ → AlLaO ₃	-0.072	-0.121	0.049
0.5K ₂ O+0.5Fe ₂ O ₃ → FeKO ₂	-0.234	-0.251	0.016
0.5K ₂ O+0.5B ₂ O ₃ → BKO ₂	-0.432	-0.457	0.025
SiO ₂ +K ₂ O → K ₂ SiO ₃	-0.421	-0.470	0.049
4SiO ₂ +K ₂ O → K ₂ Si ₄ O ₉	-0.212	-0.215	0.003
K ₂ O+2SiO ₂ → K ₂ Si ₂ O ₅	-0.317	-0.373	0.055
CrO ₃ +K ₂ O → CrK ₂ O ₄	-0.676	-0.653	-0.023
K ₂ O+2B ₂ O ₃ → B ₄ K ₂ O ₇	-0.334	-0.335	0.000
HgO+SeO ₂ → HgSeO ₃	-0.100	-0.107	0.006
SeO ₂ +CdO → CdSeO ₃	-0.178	-0.194	0.016
CaO+ZrO ₂ → CaZrO ₃	-0.059	-0.072	0.013

$\text{CaO}+\text{V}_2\text{O}_5 \rightarrow \text{CaV}_2\text{O}_6$	-0.182	-0.167	-0.016
$\text{UO}_3+\text{CaO} \rightarrow \text{CaUO}_4$	-0.182	-0.238	0.056
$\text{TiO}_2+\text{CaO} \rightarrow \text{CaTiO}_3$	-0.159	-0.171	0.012
$\text{SiO}_2+\text{CaO} \rightarrow \text{CaSiO}_3$	-0.171	-0.186	0.014
$\text{Nb}_2\text{O}_5+\text{CaO} \rightarrow \text{CaNb}_2\text{O}_6$	-0.117	-0.163	0.046
$\text{CaO}+\text{GeO}_2 \rightarrow \text{CaGeO}_3$	-0.148	-0.149	0.001
$\text{CaO}+\text{Fe}_2\text{O}_3 \rightarrow \text{CaFe}_2\text{O}_4$	-0.053	-0.035	-0.018
$\text{Cr}_2\text{O}_3+\text{CaO} \rightarrow \text{CaCr}_2\text{O}_4$	-0.070	-0.090	0.020
$\text{CuO}+\text{Cr}_2\text{O}_3 \rightarrow \text{Cr}_2\text{CuO}_4$	-0.003	-0.005	0.002
$2\text{FeO}+\text{SiO}_2 \rightarrow \text{Fe}_2\text{SiO}_4$	-0.057	-0.020	-0.037
$\text{Al}_2\text{O}_3+\text{FeO} \rightarrow \text{Al}_2\text{FeO}_4$	-0.038	-0.027	-0.011
$\text{Cr}_2\text{O}_3+\text{FeO} \rightarrow \text{Cr}_2\text{FeO}_4$	-0.072	-0.058	-0.014
$0.5\text{MoO}_2+0.5\text{MoO}_3+0.5\text{Fe}_2\text{O}_3 \rightarrow \text{FeMoO}_4$	0.020	0.006	0.014
$\text{TiO}_2+\text{FeO} \rightarrow \text{FeTiO}_3$	-0.049	-0.043	-0.006
$0.5\text{B}_2\text{O}_3+0.5\text{Rb}_2\text{O} \rightarrow \text{BRbO}_2$	-0.450	-0.440	-0.010
$\text{SiO}_2+\text{ZrO}_2 \rightarrow \text{SiZrO}_4$	-0.019	-0.026	0.006
$\text{ZnO}+\text{SeO}_2 \rightarrow \text{SeZnO}_3$	-0.093	-0.156	0.063
$\text{ZnO}+\text{Fe}_2\text{O}_3 \rightarrow \text{Fe}_2\text{ZnO}_4$	-0.033	-0.007	-0.026
$\text{ZnO}+\text{Cr}_2\text{O}_3 \rightarrow \text{Cr}_2\text{ZnO}_4$	-0.076	-0.092	0.016
$\text{Al}_2\text{O}_3+\text{ZnO} \rightarrow \text{Al}_2\text{ZnO}_4$	-0.062	-0.065	0.003
$2\text{ZnO}+\text{SiO}_2 \rightarrow \text{SiZn}_2\text{O}_4$	-0.028	-0.046	0.018
$\text{ZrO}_2+\text{SrO} \rightarrow \text{SrZrO}_3$	-0.142	-0.162	0.019
$\text{TiO}_2+\text{SrO} \rightarrow \text{SrTiO}_3$	-0.244	-0.280	0.036
$\text{SrO}+\text{SiO}_2 \rightarrow \text{SiSrO}_3$	-0.257	-0.270	0.013
$\text{SrO}+\text{MoO}_3 \rightarrow \text{MoSrO}_4$	-0.384	-0.365	-0.019
$\text{SrO}+\text{HfO}_2 \rightarrow \text{HfSrO}_3$	-0.169	-0.153	-0.016
$\text{Al}_2\text{O}_3+\text{SrO} \rightarrow \text{Al}_2\text{SrO}_4$	-0.132	-0.106	-0.026
$\text{TiO}_2+2\text{SrO} \rightarrow \text{Sr}_2\text{TiO}_4$	-0.205	-0.236	0.031
$2\text{SrO}+\text{SiO}_2 \rightarrow \text{SiSr}_2\text{O}_4$	-0.268	-0.307	0.039
$0.5\text{Cs}_2\text{O}+0.5\text{B}_2\text{O}_3 \rightarrow \text{BCsO}_2$	-0.411	-0.435	0.024
$\text{Cs}_2\text{O}+\text{UO}_3 \rightarrow \text{Cs}_2\text{UO}_4$	-0.448	-0.530	0.082
$\text{Cs}_2\text{O}+\text{MoO}_3 \rightarrow \text{Cs}_2\text{MoO}_4$	-0.574	-0.630	0.056
$\text{Cs}_2\text{O}+\text{CrO}_3 \rightarrow \text{CrCs}_2\text{O}_4$	-0.705	-0.736	0.031
$\text{TiO}_2+\text{CoO} \rightarrow \text{CoTiO}_3$	-0.062	-0.052	-0.010
$\text{CoO}+\text{SeO}_2 \rightarrow \text{CoSeO}_3$	-0.134	-0.237	0.103
$\text{Cr}_2\text{O}_3+\text{CoO} \rightarrow \text{CoCr}_2\text{O}_4$	-0.085	-0.087	0.002
$\text{SiO}_2+2\text{CoO} \rightarrow \text{Co}_2\text{SiO}_4$	-0.030	-0.018	-0.012
$0.5\text{Cr}_2\text{O}_3+0.5\text{Ce}_2\text{O}_3 \rightarrow \text{CeCrO}_3$	-0.039	-0.135	0.097
$0.5\text{Al}_2\text{O}_3+0.5\text{Ce}_2\text{O}_3 \rightarrow \text{AlCeO}_3$	0.004	-0.130	0.135
$\text{ZrO}_2+\text{BaO} \rightarrow \text{BaZrO}_3$	-0.221	-0.257	0.036
$\text{UO}_3+\text{BaO} \rightarrow \text{BaUO}_4$	-0.315	-0.378	0.063
$\text{BaO}+\text{TiO}_2 \rightarrow \text{BaTiO}_3$	-0.287	-0.320	0.033
$\text{SiO}_2+\text{BaO} \rightarrow \text{BaSiO}_3$	-0.297	-0.328	0.031
$\text{MoO}_3+\text{BaO} \rightarrow \text{BaMoO}_4$	-0.457	-0.384	-0.073
$\text{BaO}+\text{Al}_2\text{O}_3 \rightarrow \text{Al}_2\text{BaO}_4$	-0.193	-0.152	-0.040
$3\text{BaO}+\text{Al}_2\text{O}_3 \rightarrow \text{Al}_2\text{Ba}_3\text{O}_6$	-0.165	-0.181	0.017
$\text{TiO}_2+2\text{BaO} \rightarrow \text{Ba}_2\text{TiO}_4$	-0.298	-0.287	-0.011
$2\text{BaO}+\text{SiO}_2 \rightarrow \text{Ba}_2\text{SiO}_4$	-0.352	-0.392	0.039
$\text{CrO}_3+\text{Ag}_2\text{O} \rightarrow \text{Ag}_2\text{CrO}_4$	-0.145	-0.156	0.012
$\text{SiO}_2+\text{Al}_2\text{O}_3 \rightarrow \text{Al}_2\text{SiO}_5$	0.006	-0.011	0.017
$\text{Al}_2\text{O}_3+\text{TiO}_2 \rightarrow \text{Al}_2\text{TiO}_5$	0.001	0.015	-0.014
$0.5\text{P}_2\text{O}_5+0.5\text{Al}_2\text{O}_3 \rightarrow \text{AlPO}_4$	-0.270	-0.248	-0.021
$2\text{BeO}+\text{SiO}_2 \rightarrow \text{Be}_2\text{SiO}_4$	-0.009	0.017	-0.026
$\text{Al}_2\text{O}_3+\text{BeO} \rightarrow \text{Al}_2\text{BeO}_4$	-0.019	-0.024	0.005
$\text{BeO}+3\text{Al}_2\text{O}_3 \rightarrow \text{Al}_6\text{BeO}_{10}$	-0.007	0.007	-0.014
$2\text{CaO}+\text{B}_2\text{O}_3 \rightarrow \text{B}_2\text{Ca}_2\text{O}_5$	-0.213	-0.209	-0.004
$\text{Fe}_2\text{O}_3+2\text{CaO} \rightarrow \text{Ca}_2\text{Fe}_2\text{O}_5$	-0.071	-0.050	-0.020
$2\text{CaO}+\text{P}_2\text{O}_5 \rightarrow \text{Ca}_2\text{P}_2\text{O}_7$	-0.467	-0.529	0.062
$\text{SiO}_2+2\text{CaO} \rightarrow \text{Ca}_2\text{SiO}_4$	-0.192	-0.219	0.027
$\text{V}_2\text{O}_5+2\text{CaO} \rightarrow \text{Ca}_2\text{V}_2\text{O}_7$	-0.252	-0.249	-0.003
$3\text{CaO}+\text{P}_2\text{O}_5 \rightarrow \text{Ca}_3\text{P}_2\text{O}_8$	-0.496	-0.564	0.068
$\text{Al}_2\text{O}_3+3\text{CaO} \rightarrow \text{Al}_2\text{Ca}_3\text{O}_6$	-0.035	-0.013	-0.021
$\text{B}_2\text{O}_3+3\text{CaO} \rightarrow \text{B}_2\text{Ca}_3\text{O}_6$	-0.213	-0.234	0.021
$2\text{SiO}_2+3\text{CaO} \rightarrow \text{Ca}_3\text{Si}_2\text{O}_7$	-0.181	-0.188	0.007
$3\text{CaO}+\text{V}_2\text{O}_5 \rightarrow \text{Ca}_3\text{V}_2\text{O}_8$	-0.220	-0.260	0.041
$3\text{TiO}_2+4\text{CaO} \rightarrow \text{Ca}_4\text{Ti}_3\text{O}_{10}$	-0.137	-0.185	0.048
$\text{CaO}+\text{Al}_2\text{O}_3 \rightarrow \text{Al}_2\text{CaO}_4$	-0.061	-0.027	-0.034
$2\text{Al}_2\text{O}_3+\text{CaO} \rightarrow \text{Al}_4\text{CaO}_7$	-0.057	-0.015	-0.042
$\text{CaO}+\text{B}_2\text{O}_3 \rightarrow \text{B}_2\text{CaO}_4$	-0.186	-0.178	-0.008
$2\text{B}_2\text{O}_3+\text{CaO} \rightarrow \text{B}_4\text{CaO}_7$	-0.142	-0.136	-0.007

VII. REFERENCES

-
- * current address: Institut de la Matière Condensée et des Nanosciences (IMCN)-Nanoscopic Physics (NAPS), Université Catholique de Louvain
- † Electronic address: gceder@mit.edu
- ¹ G. Ceder, G. Hautier, A. Jain, and S. P. Ong, MRS Bulletin **36**, 185 (2011).
 - ² A. R. Akbarzadeh, C. Wolverton, and V. Ozolins, Physical Review B **79**, 1 (2009).
 - ³ S. V. Alapati, J. Karl Johnson, and D. S. Sholl, Physical chemistry chemical physics : PCCP **9**, 1438 (2007).
 - ⁴ A. Jain, S.-A. Seyed-Reihani, C. C. Fischer, D. J. Couling, G. Ceder, and W. H. Green, Chemical Engineering Science **65**, 3025 (2010).
 - ⁵ Y. Duan and D. C. Sorescu, The Journal of chemical physics **133**, 074508 (2010).
 - ⁶ B. Meredig and C. Wolverton, Physical Review B **80**, 1 (2009).
 - ⁷ Y. Duan, B. Zhang, D. C. Sorescu, and J. K. Johnson, Journal of Solid State Chemistry **184**, 304 (2011).
 - ⁸ M. van Setten, G. de Wijs, V. Popa, and G. Brocks, Physical Review B **72**, 2 (2005).
 - ⁹ L. Wang, T. Maxisch, and G. Ceder, Chemistry of Materials **19**, 543 (2007).
 - ¹⁰ S. P. Ong, L. Wang, B. Kang, and G. Ceder, Chemistry of Materials **20**, 1798 (2008).
 - ¹¹ S. P. Ong, A. Jain, G. Hautier, B. Kang, and G. Ceder, Electrochemistry Communications **4**, 1 (2010).
 - ¹² J. C. Kim, C. J. Moore, B. Kang, G. Hautier, A. Jain, and G. Ceder, Journal of The Electrochemical Society **158**, A309 (2011).
 - ¹³ R. E. Doe, K. A. Persson, Y. S. Meng, and G. Ceder, Chemistry of Materials **20**, 5274 (2008).
 - ¹⁴ R. E. Doe, K. A. Persson, G. Hautier, and G. Ceder, Electrochemical and Solid-State Letters **12**, A125 (2009).
 - ¹⁵ A. N. Kolmogorov, M. Calandra, and S. Curtarolo, Physical Review B **78**, 1 (2008).
 - ¹⁶ O. Levy, R. V. Chepulskii, G. L. W. Hart, and S. Curtarolo, Journal of the American Chemical Society (2009).
 - ¹⁷ A. Kolmogorov, S. Shah, E. Margine, A. Bialon, T. Hammerschmidt, and R. Drautz, Physical Review Letters **105**, 1 (2010).
 - ¹⁸ G. Hautier, C. C. Fischer, A. Jain, T. Mueller, and G. Ceder, Chemistry of Materials **22**, 3762 (2010).
 - ¹⁹ X. Zhang, A. Zunger, and G. Trimarchi, The Journal of chemical physics **133**, 194504 (2010).
 - ²⁰ G. Hautier, A. Jain, S. P. Ong, B. Kang, C. Moore, R. Doe, and G. Ceder, Chemistry of Materials **23**, 3945 (2011).
 - ²¹ T. Mueller, G. Hautier, A. Jain, and G. Ceder, Chemistry of Materials **23**, 3854 (2011).
 - ²² G. Hautier, A. Jain, H. Chen, C. Moore, S. P. Ong, and G. Ceder, Journal of Materials Chemistry **21**, 17147 (2011).
 - ²³ G. Jóhannesson, T. Bligaard, A. Ruban, H. Skriver, K. Jacobsen, and J. Nørskov, Physical Review Letters **88**, 1 (2002).
 - ²⁴ J. Feng, R. G. Hennig, N. W. Ashcroft, and R. Hoffmann, Nature **451**, 445 (2008).
 - ²⁵ J. von Appen and R. Dronskowski, Angewandte Chemie (International ed. in English) **44**, 1205 (2005).
 - ²⁶ D. Fredeman, P. Tobash, M. Torrez, J. Thompson, E. Bauer, F. Ronning, W. Tipton, S. Rudin, and R. Hennig, Physical Review B **83**, 1 (2011).
 - ²⁷ I. E. Castelli, T. Olsen, S. Datta, D. D. Landis, S. Dahl, K. S. Thygesen, and K. W. Jacobsen, Energy & Environmental Science pp. 1–6 (2012).
 - ²⁸ F. Calle-Vallejo, J. I. Martínez, J. M. García-Lastra, M. Mogensen, and J. Rossmeisl, Angewandte Chemie (International ed. in English) **49**, 7699 (2010).
 - ²⁹ J.-R. Martinez, C. E. Mohn, S. Stølen, and R. Sondenå, Physical chemistry chemical physics : PCCP **8**, 2036 (2006).
 - ³⁰ L. A. Curtiss, K. Raghavachari, G. W. Trucks, and J. A. Pople, The Journal of Chemical Physics **94**, 7221 (1991).
 - ³¹ L. a. Curtiss, K. Raghavachari, P. C. Redfern, V. Rassolov, and J. a. Pople, The Journal of Chemical Physics **109**, 7764 (1998).
 - ³² O. Kubaschewski, C. B. Alcock, and P. J. Spencer, in *Materials Thermochemistry* (Pergamon Press, 1993), chap. 5, pp. 257–323, sixth ed.
 - ³³ M. W. Chase, *NIST-JANAF Thermochemical Tables* (American Institute of Physics, Woodbury, NY, 1998).
 - ³⁴ J. Perdew, K. Burke, and M. Ernzerhof, Physical Review letters **77**, 3865 (1996).
 - ³⁵ V. Anisimov, J. Zaanen, and O. Andersen, Physical Review B **44**, 943 (1991).
 - ³⁶ V. I. Anisimov, F. Aryasetiawan, and A. I. Lichtenstein, Journal of Physics: Condensed Matter **9**, 767 (1997).
 - ³⁷ L. Wang, T. Maxisch, and G. Ceder, Physical Review B **73**, 1 (2006).
 - ³⁸ G. Kresse and J. Furthmuller, Computational Materials Science **6**, 15 (1996).
 - ³⁹ P. Blöchl, Physical Review B **50**, 17953 (1994).
 - ⁴⁰ A. Jain, G. Hautier, C. J. Moore, S. P. Ong, C. C. Fischer, T. Mueller, K. A. Persson, and G. Ceder, Computational Materials Science **50**, 2295 (2011).
 - ⁴¹ G. L. W. Hart and R. W. Forcade, Physical Review B **77**, 1 (2008).
 - ⁴² W. Setyawan and S. Curtarolo, Computational Materials Science **49**, 299 (2010).
 - ⁴³ W. Setyawan, R. M. Gaume, S. Lam, R. S. Feigelson, and S. Curtarolo, ACS combinatorial science (2011).
 - ⁴⁴ ICSD, *Inorganic Crystal Structure Database* (2006).
 - ⁴⁵ Thermochemistry, *Landolt-Bornstein Database* (2011).
 - ⁴⁶ [Http://www.ctdp.org/](http://www.ctdp.org/).

- ⁴⁷ E. G. King, *Journal of Physical Chemistry* **60**, 410 (1956).
- ⁴⁸ X. Ke and A. Kuwabara, *Physical Review B* pp. 2–8 (2005).
- ⁴⁹ Z.-g. Mei, Y. Wang, S.-l. Shang, and Z.-k. Liu, *Inorganic Chemistry* (2011).
- ⁵⁰ See supplemental material at [url will be inserted by publisher] for cif files of the $gga(+u)$ relaxed structure in their fm state.
- ⁵¹ C. Franchini, R. Podloucky, J. Paier, M. Marsman, and G. Kresse, *Physical Review B* **75**, 1 (2007).
- ⁵² S. Lany, *Physical Review B* **78**, 1 (2008).
- ⁵³ D. G. Pettifor, *Journal Of The Chemical Society Faraday Transactions* **86**, 1209 (1990).
- ⁵⁴ N. Skorodumova, R. Ahuja, S. Simak, I. Abrikosov, B. Johansson, and B. Lundqvist, *Physical Review B* **64**, 1 (2001).
- ⁵⁵ C. Loschen, J. Carrasco, K. Neyman, and F. Illas, *Physical Review B* **75**, 1 (2007).
- ⁵⁶ R. Ahuja, A. Blomqvist, P. Larsson, P. Pykkö, and P. Zaleski-Ejgierd, *Physical Review Letters* **106**, 1 (2011).
- ⁵⁷ T. Lindemer, T. Besmann, and C. Johnson, *Journal of Nuclear Materials* **100**, 178 (1981).
- ⁵⁸ T. Mathews, D. Krishnamurthy, and T. Gnanasekaran, *Journal of Nuclear Materials* **247**, 280 (1997).
- ⁵⁹ P. A. G. O’Hare, *The Journal of Chemical Thermodynamics* **6**, 425 (1974).
- ⁶⁰ N. Shukla and R. Prasad, *The Journal of Chemical* **25**, 429 (1993).
- ⁶¹ Z. Singh, S. Dash, and R. Prasad, *Journal of alloys and* **279**, 287 (1998).
- ⁶² A. Olin, *Chemical thermodynamics of selenium, Volume 1* (Elsevier, 2005), ISBN 0444514031.
- ⁶³ Y. Tardy and P. Vieillard, *Contributions to Mineralogy and Petrology* **63**, 75 (1977).
- ⁶⁴ S. R. Eliason, *Maximum Likelihood Estimation: Logic and Practice* (Sage Publications, Inc, 1993), ISBN 0803941072.
- ⁶⁵ B. Efron and D. Hinkely, *Biometrika* **65**, 457 (1978).
- ⁶⁶ [Http://www.materialsproject.org/](http://www.materialsproject.org/).
- ⁶⁷ A. Jain, G. Hautier, S. P. Ong, C. Moore, C. C. Fischer, and G. Ceder, *Physical Review B* **84**, 045115 (2011).
- ⁶⁸ Y. Mo, S. Ong, and G. Ceder, *Physical Review B* **84**, 1 (2011).
- ⁶⁹ J. Heyd, G. E. Scuseria, and M. Ernzerhof, *The Journal of Chemical Physics* **118**, 8207 (2003).
- ⁷⁰ R. Armiento and A. Mattsson, *Physical Review B* **72**, 1 (2005).
- ⁷¹ A. Mattsson and R. Armiento, *Physical Review B* **79**, 1 (2009).
- ⁷² V. L. Chevrier, S. P. Ong, R. Armiento, M. K. Y. Chan, and G. Ceder, *Physical Review B* **82**, 075122 (2010).
- ⁷³ W. Foulkes, L. Mitas, R. Needs, and G. Rajagopal, *Reviews of Modern Physics* **73**, 33 (2001).
- ⁷⁴ Debye temperature, heat capacity, density, melting and boiling points, *Landolt-Bornstein Database* (2011).
- ⁷⁵ H. Flotow and D. Osborne, *The Journal of Chemical Thermodynamics* **6**, 135 (1974).
- ⁷⁶ S. Stolen, R. Glockner, F. Gronvold, A. Tooru, and S. Izumisawa, *American Mineralogist* **81**, 973 (1996).
- ⁷⁷ For instance, we found during our investigation that the “Mo” PAW pseudopotentials provided by VASP led to much larger errors for some reaction energies (e.g., $\text{Na}_2\text{O}+\text{MoO}_3\rightarrow\text{Na}_2\text{MoO}_4$) than if the “Mo_pv” pseudopotential, including the p -electrons as valence electrons, was used.